Research article

Translaminar neuromorphotopological clustering and classification of dentate nucleus neurons

Ivan Grbatinić[1,*], Nebojsa Milosevic[1], Dusica Maric[2]

[1] *Laboratory for digital image processing and analysis, Institute of Biophysics, Medical Faculty, University of Belgrade, 11000 Belgrade, Serbia*
[2] *Institute of Anatomy, Medical Faculty, University of Novi Sad, Serbia*

***Correspondence**: igrbson@gmail.com (Ivan Grbatinić)

https://doi.org/10.31083/JIN-170044

Abstract

This study aims to determine whether dentate neurons can be translaminarly neuromorphotopologically classified as ventrolateral or dorsomedial type. Adult human dentate interneuron 2D binary images are analyzed. The analysis is performed on both real and virtual neuron samples and 29 parameters are used. They are divided into the classes: neuron surface, shape, length, branching and complexity. Clustering is performed by an algorithm that employs predictor extraction (matrix attractor analysis/non-negative matrix factorization and cluster analysis of predictor factors – separate unifactor analysis/Student's t-test and MANOVA) and multivariate cluster analysis (cluster analysis, principal component analysis, factor analysis with pro/varimax rotation, Fisher's linear discriminant analysis and feed-forward backpropagation artificial neural networks). The separate unifactor analysis extracted as significant the following predictors from the natural cell sample: the $N_{pd}(p < 0.05)$, and from the virtual cell sample: the Adt ($p < 0.05$), $D_o(p < 0.001)$, $M_s(p < 0.01)$, $D_{wdth}(p < 0.001)$, $N_{pd}(p < 0.05)$, $N_{sd}(p < 0.001)$, $N_{t/hod}(p < 0.001)$, $N_{\max}(p < 0.01)$, $D_s(p < 0.001)$, $C_{df}(N_{t/hod})_{st}(p < 0.05)$. For the multidimensional analysis, with the exception of the Fisher's linear discriminant analysis which gave a false positive result, all other analyses rejected the translaminar dentate neuron classification. Thus, dentate neurons cannot be classified into ventrolateral/dorsomedial neuromorphotopological subtypes. Although some differences were found to exist, they are not sufficient to carry this classification. The methods of multidimensional statistical analysis are again shown to be the best for such kinds of analysis.

Keywords

Dentate neurons; 2D binary image; translaminar neuromorphotopological clustering/classification based upon un/supervised learning techniques; parameter; multidimensional analysis; Fisher's linear discriminant analysis; multidimensional approach

Submitted: May 4, 2017; **Accepted:** August 8, 2017

1. Introduction

The dentate nucleus (dentatus) is positioned in a central region of the white matter of the cerebellum. Its main role is as a distribution (relay) center for neural pathways coming from the Purkinje neurons of the cerebellum [1]. Phylogenetically, it is the youngest and largest of all the cerebellar nuclei and serves as the main pathway-crossing relay center between other parts of the brain and the cerebral cortex. It receives afferents from the supplementary motor and premotor neocortex via pontocerebellar areas. Crossing over at the pontomesencephalic junction, its efferent pathways, the dentatus, project via the superior peduncle through the rubral nucleus to the ventrolateral thalamic nuclei. The dentate nucleus is involved in the processes of planning, initiation, and control of volitional movement [2].

During development of the human DN, neuroprecursors that will form the pool of mature neurons of the adult nucleus take their final positions at gestation week 12.5 [3]. The DML continues its development until gestation week 19.5. This occurs after precursors of the small and large neurons are formed [3]. At that time neural precursors of the VLL start to increase their size [3]. The peak of VLL elongation is reached at the 23th week of gestation and the beginning of folding is observed after a week and a half (23.5th gestation week).

With regard to the question of neuronal distribution across the lamina, Maric [4] found a uniform distribution of all neuronal types in both laminae. The small neurons are uniformly scattered throughout the nucleus in the DML as well as in the VLL. Two types of border neurons are arranged predominantly along the inner and the outer quarter of both lamina. The interesting fact is that similarly to border neurons, central neurons are also characterized by the same uniform arrangement in both lamina i.e. along their inner two quarters. Thus, for all neuronal types there are no differences in translaminar arrangement [4].

Consideration of these reports suggest that the indices for neurons belonging to these laminas should be histologically different. Since previous studies have shown the characteristics and potential classifications of central and border neuron types, the possibility of histological clustering and classification based on topological criteria is investigated. In other words, can DN neurons be translaminarly neuromorphotopologically classified using methods of multidimensional analysis. In a previous study dealing with the neuromorphological computational response surface methodology (RSM) modeling of DN neurons differently structured translaminar models were explored [5].

The aim now is to determine whether these differences are significant and sufficient to classify neurons accordingly. Additionally,

by introducing matrix attractor analysis, the second, methodological, aim is to further develop the previously described [6] classification algorithm.

2. Materials and methods

The adult human dentate nucleus (DN) is characterized by two phylogenetically different parts, the younger ventrolateral lamina (VLL) and older dorsomedial lamina (DML) (Fig. 1).

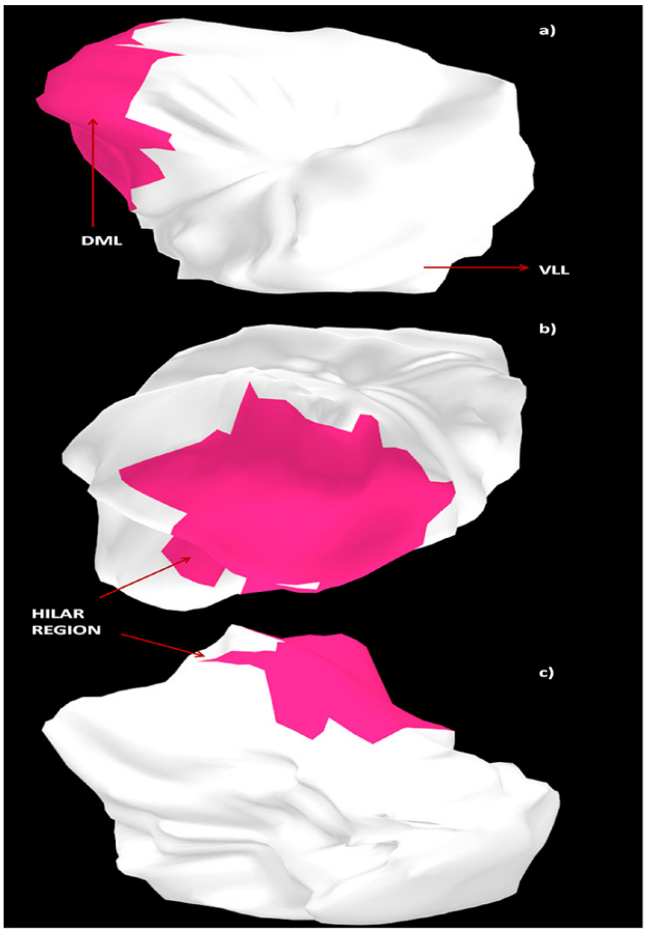

Fig. 1. 3D reconstruction of the dentate nucleus together with its laminar structure. (a) dorsolateral view, (b) anteromedial view, (c) inferomedial view. From these three panels it can be seen that the DML occupies a much smaller proportion of the nucleus when compared with the VLL.

The illustrations of the nucleus (1846) didn't show these parts of the nucleus to be different [7], but Gans [8] identified differences when measuring the size of neurons in these two nuclear compartments early in the twentieth century. The DML is the so called paleodentatus and is homologous with the lateral cerebellar nucleus of lower species. The VLL represents the neodentatus which comprises the majority of the nucleus in higher primates and humans. During fetal development the neurons of the DML lamina can be seen to be larger than the neurons of the VLL. Therefore, the DML lamina is referred to as the magnocellular component of the nucleus while the VLL comprise its parvocellular part [9, 10].

2.1. *Impregnation procedure and acquisition of a 2D neuron binary image*

Material used in this study was collected during the period 2013–2014 at the Department of Forensic Medicine, School of Medicine, University of Novi Sad (Serbia), with the approval of the Ethics Committee of the University of Novi Sad, School of Medicine (Serbia). Independently of gender and side of the brain, the tissue samples of the dentate nuclei were taken from 30 brains, 24 male and 6 female, with an age range of 32–88 years old. Tissue samples were taken from cadavers with undamaged brains and without diagnosed cerebro/cardiovascular or nervous system disease. Independently of the side, dentate nuclei were cut into slices 2.5 mm thick then fixed using the KopschBubenaite impregnation technique [11]. Afterwards tissue blocks embedded in paraffin were dehydrated by immersion in increasing alcohol concentrations. Serial horizontal sections were cut (90 μm thick) and mounted on glass slides.

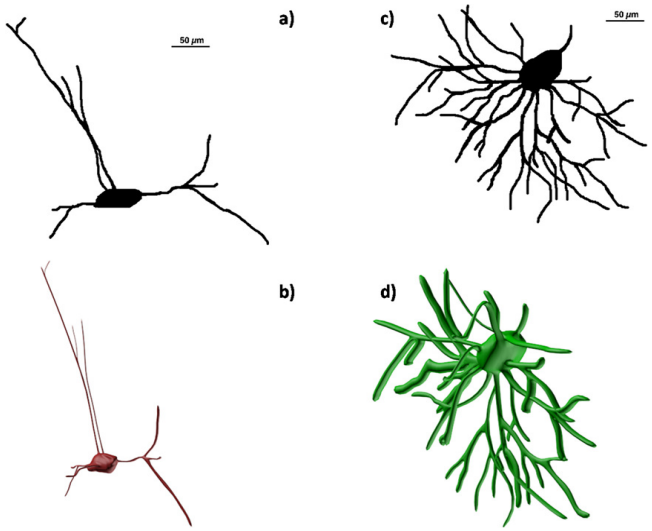

Fig. 2. Representative neurons from the laminae of the dentate nucleus. (a) 2D binary image of VLL neuron, (b) 3D reconstructive image of VLL neuron, (c) 2D binary image of DML neuron, (d) 3D reconstruction DML neuron.

Using light microscope magnification (x400), each slide was observed in detail. Impregnation of slide samples was considered successful when the region of interest showed a number of impregnated neurons throughout the series of sections. Neuron images were recorded and digitally transformed by digital camera "Leica DC 100" (Leica Microsystem Wetzlar GmbH, Wetlzar, Germany) with accompanying software (Leica Microsystem Wetzlar Ltd., Heerbrug, Switzerland). An image of each neuron was obtained by first scanning it from six image slices by increasing the focal depth (15 μm). These partial neuron images were then imported into software specialized for digital image analysis and reconstruction: Image J (http://www.rsb.info.nih.gov/ij). Using the command *ZProject*, all neuron images are projected onto a stack axis normal to the image plane, while dendrite spines, axons, and background artifacts, were digitally removed. The image obtained was a black 2D binary digital neuron image on a white background (Fig. 2a and 2c).

2.2. *The neuromorphological computational parameters*

This study employed 29 computational parameters that described various aspects of neuron morphology. They were divisible into the following categories: (1) neurocompartmental surface, (2) neuron shape, (3) neuron compartmental length, (4) dendritic arborization branching, and (5) computational neuromorphological complexity. These were the main parameter classifications used for this study. The majority of parameters were unstandardized (21 of 29). Comparisons based on unstandardized parameters are more integrative due to the large amount of noise confounding hidden in the data and are more realistic but less revealing in terms of a single factor of influence in the determination of DN inter-laminar differences. Thus, to more accurately perform inter-laminar comparisons, in terms of single factors, standardized parameters of neuron morphology (8) are also introduced in this study. They provide ratios for some parameters. To summarize, unstandardized parameters allow more holistic inter-factor interplay than standardized factors which are more successful in revealing the influence of any one factor on neuron classification.

To keep track of the final classification result, details of parameter derivation and calculation are given in an Appendix. For completeness, derivations are summarized in Table 1 and parameter abbreviations are defined in the Appendix.

Table 1. Derivation and calculation of neuromorphological computational parameters of DN neurons

Parameter	Method	Formula
A_s	Direct digital measuring	/
A_n	Direct digital measuring	/
A_{dt}	Derivation	$A_{dt} = A_n - A_s$
A_{nf}	Direct digital measuring	/
A_{df}	Derivation	$A_{df} = A_{nf} - As$
A_{pns}	Derivation	$A_{pns} = A_{df} - A_{dt}$
L	Skeletonization	/
r_c	Fractal	/
r_b	Numbering	/
r_t	Numbering	/
D_{wdth}	Derivation	$D_{wdth} = \frac{A_{dt}}{L}$
D_o	Fractal	/
M_S		$M_s = \frac{PR_s^2}{4\pi \cdot A_s}$
M_n		$M_n = \frac{PR_N^2}{4\pi \cdot A_n}$
N_{dall}	Derivation	$N_{dall} = N_{pd} + N_{sd} + N_{t/hod}$
N_{pd}	Numbering	/
N_{sd}	Numbering	/
$N_{t/hod}$	Numbering	/
$N_{\max}$	Fractal	/
D_s	Fractal	/
C_{df}	Fractal	/
L_{st}	Derivation	$L_{st} = \frac{L^2}{A_s}$
$(D_{wdth})_{st}$	Derivation	$(D_{wdth})_{st} = \frac{D_{wdth}^2}{A_s}$
$(r_c)_{st}$	Derivation	$(r_c)_{st} = \frac{r_c^2}{A_s}$
$C_{df}(A_{df})_{st}$	Derivation	$C_{df}(A_{df})_{st} = \frac{C_{df}}{A_{df}}$
$C_{df}(N_{dall})_{st}$	Derivation	$C_{df}(N_{dall})_{st} = \frac{C_{df}}{N_{dall}}$
$C_{df}(N_{pd})_{st}$	Derivation	$C_{df}(N_{pd})_{st} = \frac{C_{df}}{N_{pd}}$
$C_{df}(N_{sd})_{st}$	Derivation	$C_{df}(N_{sd})_{st} = \frac{C_{df}}{N_{sd}}$
$C_{df}(N_{t/hod})_{st}$	Derivation	$C_{df}(N_{t/hod})_{st} = \frac{C_{df}}{N_{t/hod}}$

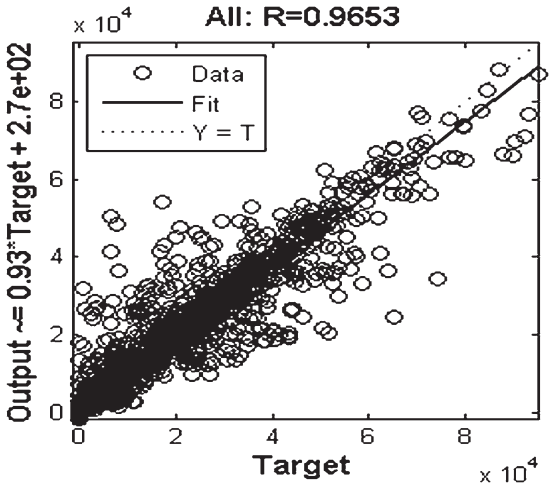

Fig. 3. Linear regression analysis gives excellent NARX ANN performance for data extrapolation used in real sample enlargement and thus generation of the semi/virtual DN sample.

2.3. *The DN neuron samples*

The entire dataset of 337 neurons consisted of two DN sample groups, i.e., VLL and DML. The real VLL sample comprised 152 (45.1%) neurons while the virtual DML sample contained 185 (54.9%) neurons. In this study, a virtual DN sample using the NARX/NAR neural network [12] was employed due to the potentially small sample size for the defined task and to validate results for larger (virtual) samples. Thus, the virtual sample is actually semi-virtual as it contained both real and computationally formed (virtual) neuron data. The structure of the virtual sample was: 190 (14.16%) DML neurons and 1152 (85.84%) VLL neurons, for a total of 1342 semi-virtual neurons. Any arbitrary choice of the NARX/NAR ANN parameters led to such a sample structure despite varying but universally high performance levels (Fig. 3). These two samples were analyzed separately for the given parameters.

2.4. *Statistical data analysis*

Data were analyzed using nonnegative matrix factorization (NMF) and cluster analysis of factor predictors (PFCLA) as parts of the matrix attractor analysis. Subsequently, PCA and factor analyses with promax/varimax rotation was undertaken, followed by a Fisher's multiple linear discriminant analysis (FMLDA), the two layer feed-forward backpropagation artificial neural network (ANN), along with Kohonen's self-organizing map (SOM), cluster analysis, Student's *t*-test, and a factorial design two-way multivariate analysis of variance (MANOVA) as part of a separate unifactor analysis. The data analysis of the Gaussian distribution pattern was performed using the Kolmogorov–Smirnov and Shapiro–Wilk tests.

3. Results

3.1. *Preliminary stochastic matrix attractor analysis/NMF and PFCLA analysis*

The translaminar VLL/DML neuromorphotopological clustering of DN neurons was initiated with a matrix attractor analysis comprised of NMF and PFCLA analysis (Fig. 4).

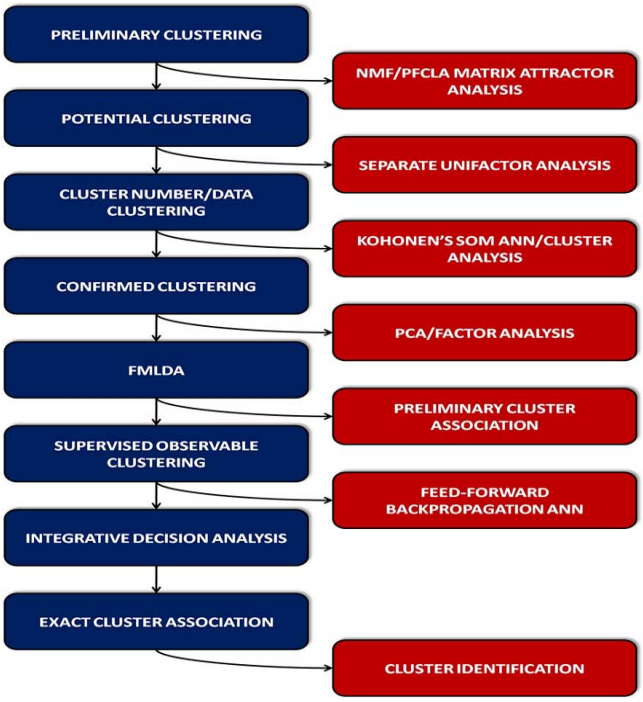

Fig. 4. Flux diagram of the general neuron clustering applied to neurons from the dentate nucleus.

Analysis extracted dominant clustering predictors at the level of the entire data set for which it was expected to provide one of the major driving forces. The NMF analysis is a dimension-reduction technique based on a low-rank approximation of the feature space. Besides providing a reduction in the number of features, NMF guarantees that the features are positive, producing additive models that respect the non-negativity of physical quantities. For a sample matrix, in the present case a DN neuron matrix, it finds two matrices W and H as its computational matrix predictors. By further analysis of these two matrices the real factor/predictors can be extracted [13, 14]. The PFCLA is an ordinary hierarchical cluster analysis but with factors as the objects of clustering. It is expected that these two analyses would have different results when applied to the same data, but with some common overlap. If such overlap exists, then the factors creating it would represent the dominant driving forces stabilizing the system (attractors of a system) and would be candidates for clustering if they existed.

For the real DN sample, NMF analysis extracted as dominant attractors of the DN neuron sample the A_{nf}, A_{df}, and the A_{pns} parameters (Fig. 5a). The same result was obtained for the virtual sample (Fig. 5b). PFCLA also extracted the same significant factors. The inter-grouping average linkage method on the real sample revealed two major clusters of factors: the first with the three aforementioned predictors, the second with the remaining factors (Fig. 6a). Again, A_{nf} was found to be the strongest factor (factor strength about 10) while A_{df} and the A_{pns} belonged to the same sub-cluster with the same descending order by strength, 10 and 6, respectively. Though A_{nf} and A_{df} share the same level of strength, the A_{nf} was the strongest due to its singularity. The within-grouping average linkage method revealed the same result but the three factors exhibited the same order of descending power (Fig. 6b). The situation was identical for the virtual sample (Fig. 6c and 6d). Thus, the cross-section between the NMF and PFCLA analyses was the full set of extracted factors i.e. the full match. According to these results it is expected that successful clustering will be obtained and that these factors will play the major role in the clustering of DN neurons.

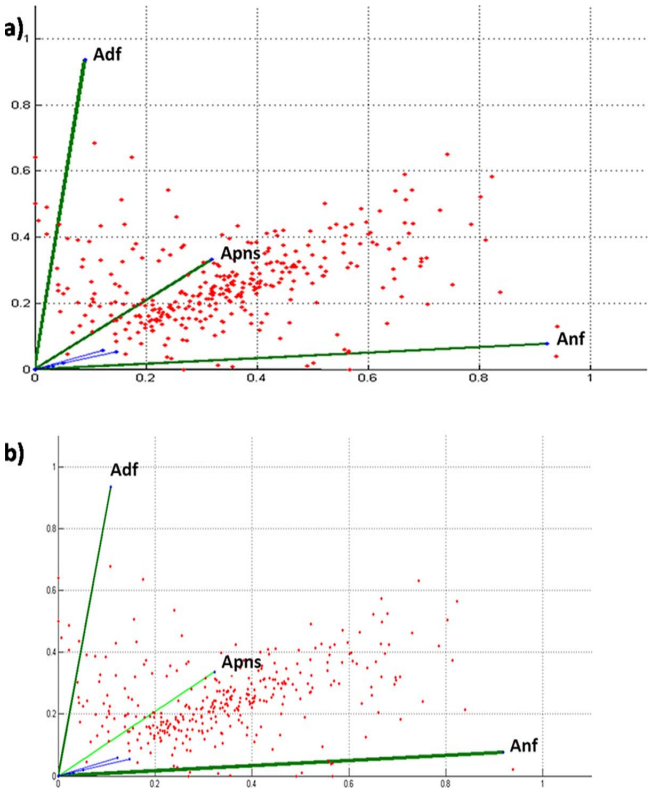

Fig. 5. NMF analysis biplot. (a) NMF analysis of the real DN neuron sample dataset. Graph shows the entire DN neuron sample dataset is a single elongated cluster with the three dominant driving factor/predictor forces/attractors: Anf (factor strength of influence 92.17%), Adf (93.62%) and $Apns$ (33.29%). With the exception of a few outliers, as the greatest width and density of the cluster is at its center, the NMF analysis does not indicate DN translaminar VLL/DML clustering. (b) NMF analysis on the virtual DN neuron sample dataset shows an identical result, negligible and insignificant variation, as for the real sample (colors and line widths represent relative factor strengths).

3.2. *Potential clustering/separate unifactor analysis*

A separate unifactor analysis is based upon the Student's t-test and factorial design two-way MANOVA. On the real sample it extracted, as relevant for the DN neuron classification, one of the observed parameters: the $N_{pd}(p < 0.05)$ (Table 2, Fig. 7–Fig. 11). On the virtual sample (Table 3, Fig. 7–Fig. 11) the significant parameters are: the $A_{dt}(p < 0.05)$, $D_o(p < 0.001)$, $M_s(p < 0.01)$, $D_{wdth}(p < 0.001)$, $N_{pd}(p < 0.05)$, $N_{sd}(p < 0.001)$, $N_{t/hod}(p < 0.001)$, $N_{\max}(p < 0.01)$, $D_s(p < 0.001)$, $C_{df}(N_{t/hod})_{st}(p < 0.05)$. The Student's t-test and MANOVA showed the same clustering factors for both real and virtual neuron samples in terms of the extracted relevant parameters. It can be seen from the Table 2 and Fig. 7–Fig. 11 that DML neurons approximately have more developed dendritic branching than VLL neurons but a smaller complexity level of shape and dendritic arborization. Fig. 2a and 2c shows extreme

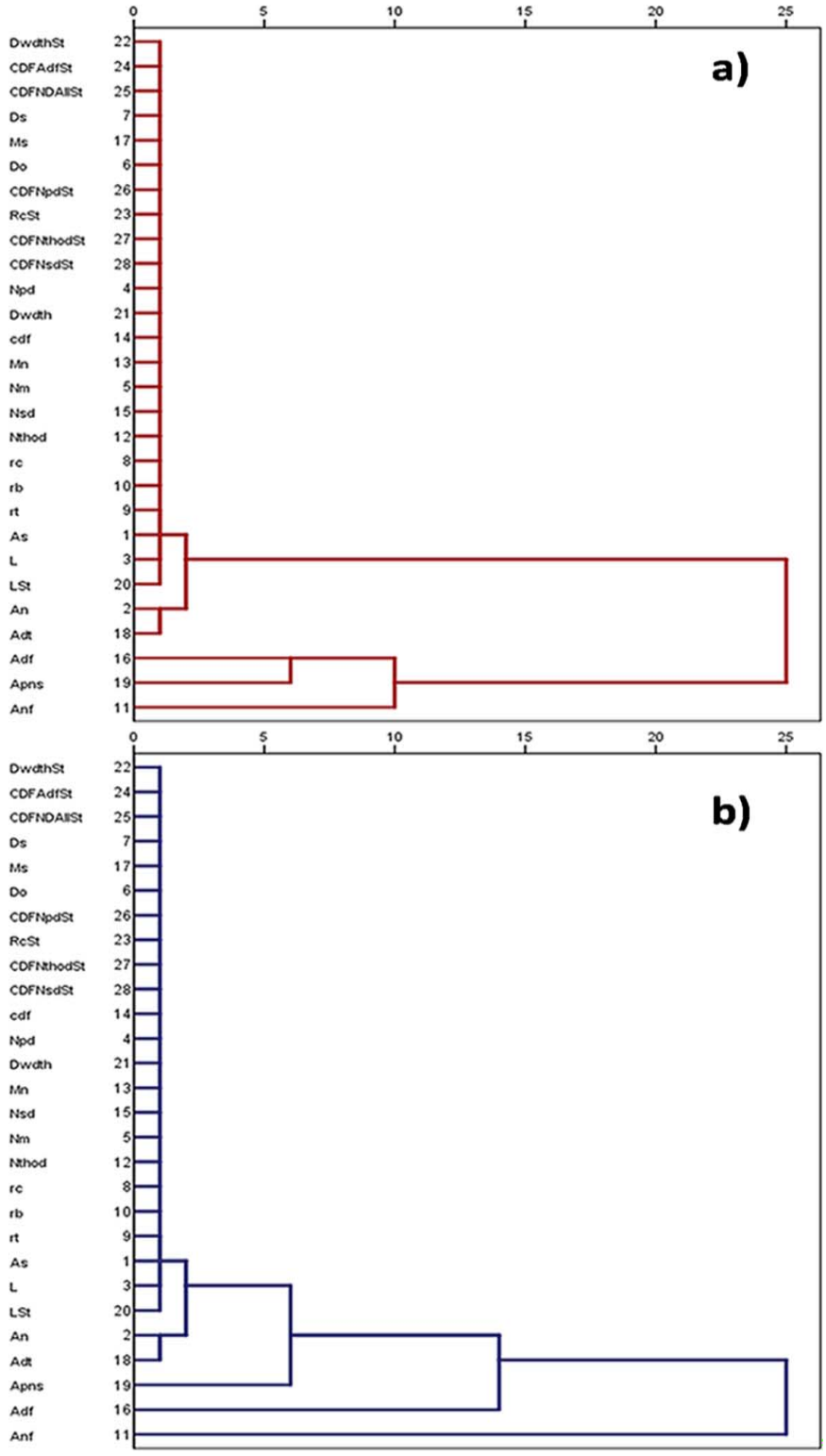

Fig. 6. Dendrograms of hierarchical cluster analysis of factors. (a) and (b) PFCLA obtained for the natural DN sample dataset. (a) Inter-group average linkage method shows predictors Anf and Adf to represent a one factor cluster with a factor/cluster strength level of about 10 with the lower level $Apns$ (factor strength about 7) within that predictor cluster as a branch of an Adf sub-cluster. (b) Consistent with the foregoing, the within-group average linkage method shows that the predictors Anf , Adf , and $Apns$ have the strongest respectively decreasing factor/cluster strength – the Anf as the strongest represents the sub-cluster for itself, while the other two following it are second and third sub-clusters, respectively (note similarity with results of the NMF analysis). Both diagrams show a dispersed and thus negligible effect of the other factors making the second predictor cluster. Their vanishing resultant effect over the data clustering is much better explained and demonstrated by the NMF analysis vector diagram.

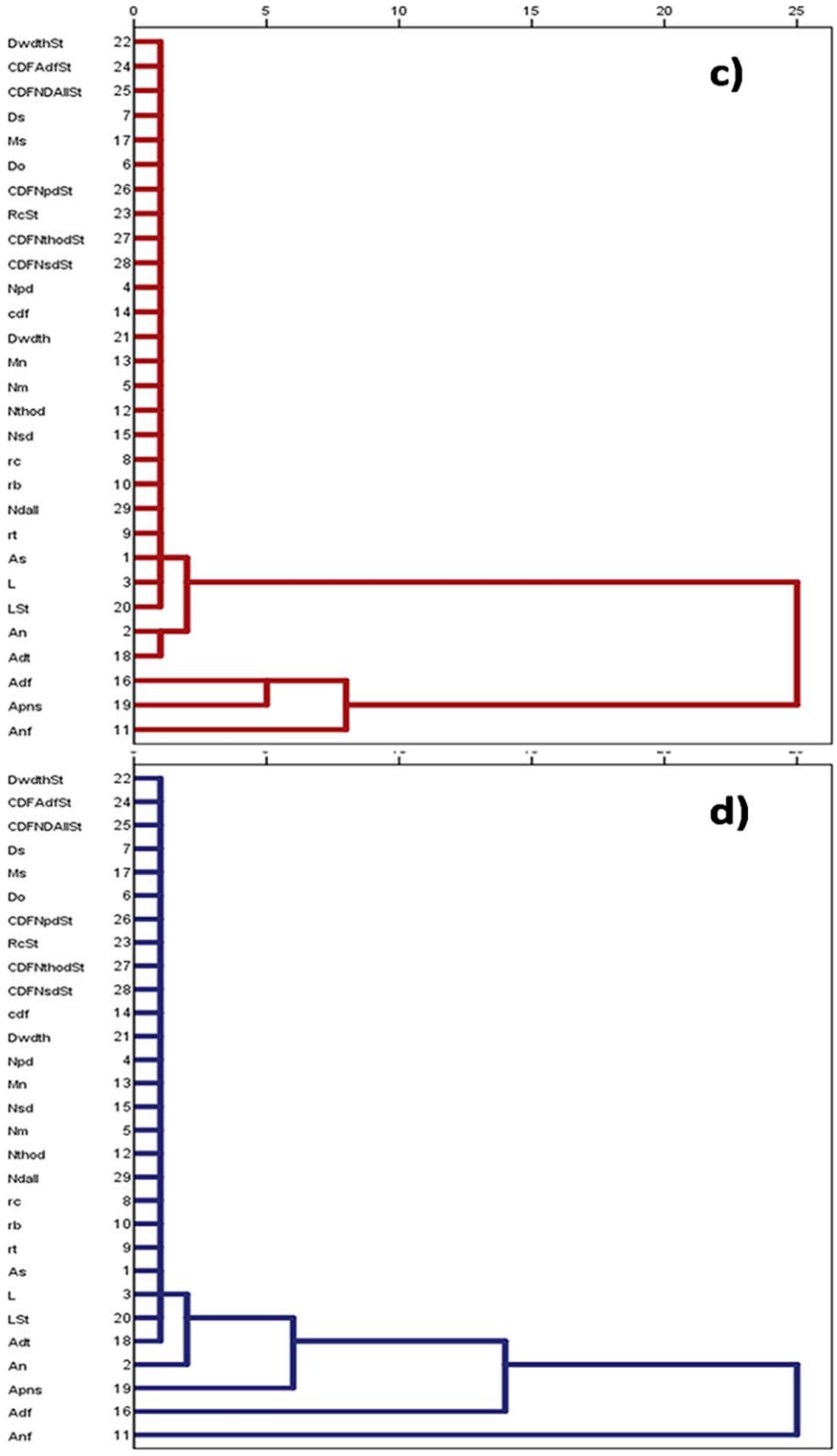

Fig. 6. (Continued.) (c) and (d) PFCLA obtained on the virtual DN sample dataset is identical to the real sample (axes signify parameters).

representatives from each group at the end of parameter distributions to show how these neurons can be different despite the fact that they actually belong to the same type as revealed by analysis. Differences are very obvious but to further increase this difference, 3D reconstruction of 2D binary images were used (Fig. 2b and 2d). It should be emphasized that although unifactor analysis extracts different factors from the samples, it cannot show whether interaction of number and strength of such differences is sufficient to successfully cluster the data. Thus, to determine this, multidimensional analysis was employed.

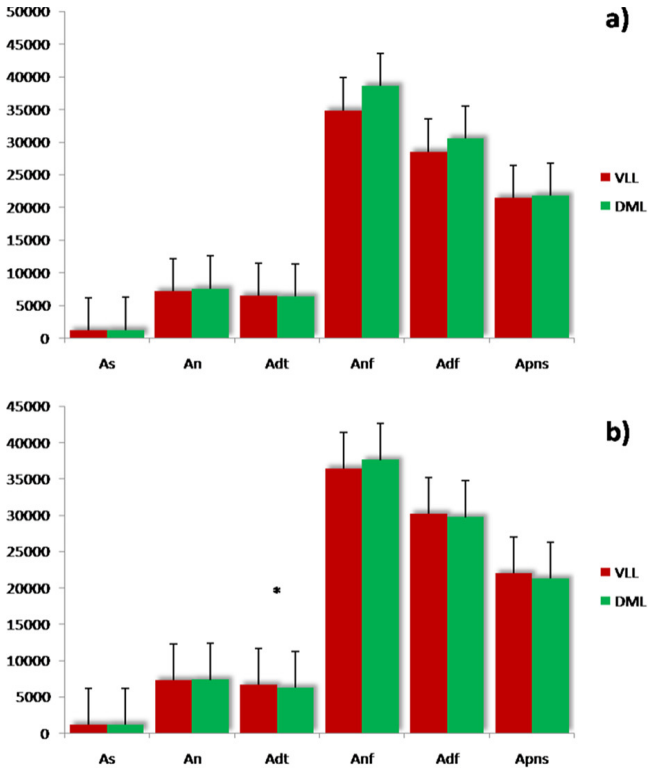

Fig. 7. Surface morphometric parameters of DN neurons; ∗ statistically significant ($p < 0.05$).

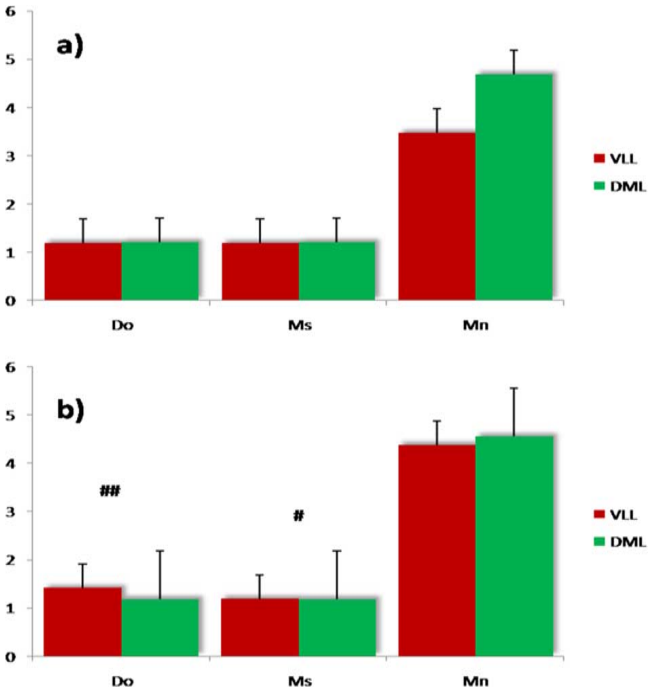

Fig. 8. Shape morphometric parameters of DN neurons; # highly significant ($p < 0.01$); ## very highly significant ($p < 0.001$).

3.3. Cluster number determination/Kohonen's SOM ANN and cluster analysis

Cluster analysis provides a classification tool that uses parametrical multivariate data. It is based on identification of the dominant multi-parameter attractor values of clusters in a sample, so called cluster centers. Clustering is thus performed using estimation of the degree of separation between clusters i.e. it is based on determining so-called Euclidian inter-cluster distances (ED). Depending upon this value, the existence of clusters may or may not be established [15]. The SOM is an ANN with matrix representation of neurons where each neuron has the possibility of representing single cluster centers. This neuron is referred to as the cardinal neuron and carries the majority of the observables, in this case, the DN neurons. Analogously to cluster analysis, inter-cluster distances are then calculated between given cluster centers/cardinal neurons [16]. Thus, similarly to the cluster analysis, the SOM can be considered to represent some kind of an ANN based cluster analysis. In this study three types of cluster analysis are performed: *k*-means, two-step, and hierarchical. The *k*-means cluster analysis is used to find the best inter-cluster separation obtained for the three clusters on the real sample. The ED 1/2 is 2.53 104, ED 1/3 3.42 104, ED 2/3 5.95 104 and the number of neurons in each cluster is 150 (cluster I 44.51%), 136 (cluster II 40.36%), and 51 (cluster III 15.13%). The average ED is 3.97 104. The two cluster solution: ED 1/2 is 3.76 104 and the number of neurons in each cluster is 228 (67.66%) in cluster I and 109 (32.34%) in cluster II. The comparison of the ED 1/2 in the two-cluster solution with the average ED in the three-cluster solution suggests that the three-cluster solution as better due to larger inter-cluster distances which confirm better cluster separation in that case. Additionally, according to beta-error, for the clustering be successful, the number of neurons/observables in each of the obtained clusters cannot exceed 20% of the ideal theoretical 50%/ 50% distribution in the case of the two-cluster solution i.e. 33.33% in the three-cluster solution. In the case of the given two-cluster solution obtained from the real DN sample, the maximally allowed neuron distribution across the clusters is 51 neurons (15%) (the minimal number) in one cluster and 286 (85%) (the maximal number) in the other cluster. Since both clusters satisfy the given limits, clustering in the absolute sense is validated and the data are open to further analysis. For the three-cluster solution, the maximal possible asymmetry of cluster structure is 34 (9.9%) neurons for two clusters and 269 (90.1%) for the third cluster. Thus, this cluster solution is also valid, so the two solutions obtained for the real DN sample can be compared in terms of the number of neurons in each cluster. The larger average ED distance in the three-cluster solution leads to one of two possible outcomes: either one of the two clusters in the two-cluster solution is broken onto two sub-clusters in the three-cluster solution or it is not, i.e. neurons are clustered again with the total cluster reset without preserving one of the clusters. In order to know which is correct, the concept of beta-error is again employed, but now as the allowed SD value for the number of neurons in each cluster identified for the two-cluster solution. Analysis revealed that none of the combinations of two of the clusters in the three-cluster solution leads to the clusters of the two-cluster solution thus supporting the latter outcome. The neurons are clustered through the total reset without either preservation of one cluster or the break-down of the other. This supports the extreme similarity of neuron morphology and the absence of any possibility of classification. The reasons for the classification failure for DN

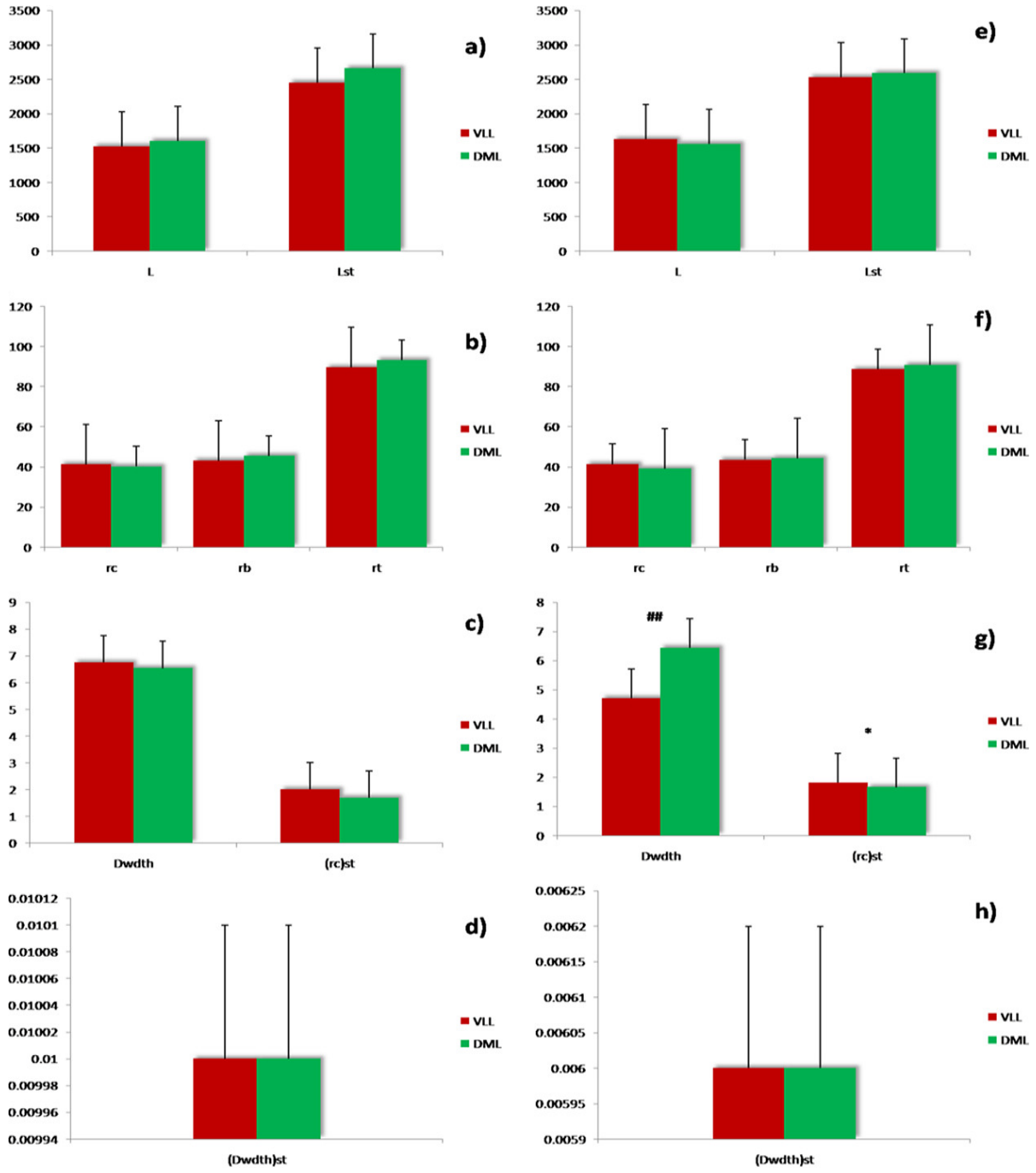

Fig. 9. Length morphometric parameters of DN neurons; statistically significant ($p < 0.05$); ## very highly significant ($p < 0.001$) adjacent plots with the same parameter sets represent real (red–left) and virtual samples (green–right).

neurons are: (1) Average ED in the three-cluster solution is larger than for the two-cluster solution, (2) The three-cluster solution is more valid than the two-cluster solution due to more uniform neuronal distribution across clusters, and (3) Neurons remain clustered through the total cluster reset, thus confirming their own neuromorphological similarity. Although this conclusion is not necessarily due to any obvious failure of the two-cluster solution, as it is only based on and ED comparison, it was undertaken to determine how deeply the clustering failure goes, i.e. due to its semi-quantification. The outcome for the virtual sample is identical to that of the real one, even with a stronger three-cluster solution, in terms of both ED differences and neuron inter-cluster distribution. Two step cluster analysis of the real sample also showed a three-cluster solution with a cluster strength of about 38% (reasonable clustering). For the virtual sample it provided only an one cluster solution. This inconsistency also shows the clustering failure for DN neurons. Hierarchical cluster analysis confirmed the absence of clustering for both samples, real and virtual (Fig. 12). Kohonen's SOM was consistent with the results

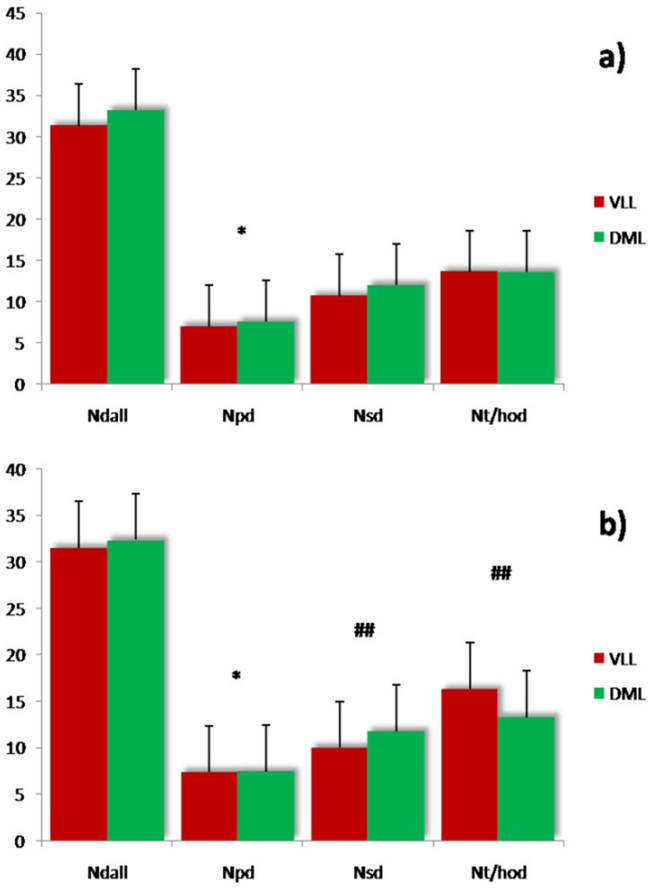

Fig. 10. Branching morphometric parameters of dendritic tree of DN neurons; statistically significant ($p < 0.05$); ## very highly significant ($p < 0.001$).

of the cluster analysis (Fig. 13 and Fig. 14).

3.4. *Confirmation of clustering absence/PCA and factor analysis*

PCA analysis followed by factor analysis with promax/varimax rotation was employed. The reasons for this include, (1) The particular ability to potentially cluster data, if possible, and (2) Multivariate data reduction together with the ability to reveal predictor/factor groups as vectors that separate neurons into groups/clusters along the main principal components that explain and carry the majority of data variance, thus determine neuromorphology [17]. This implies that besides classification of observables, in this case neurons, these analyses also may serve in parallel as predictor cluster analyses. The analysis was undertaken on the parameter correlation matrix. Optimal loadings were obtained by rotating the three principal components [18, 19]. For each of the samples it was observed that the consistency of its situation was reflected in its complete irregularity, i.e. in each case, an absence of any clustering pattern. Although the majority of data variability captured was constantly above 51% with three principal components, the inter-methodological and inter-sample variances in factor loadings and orientation determining pseudo/clusters was extremely variable, thus removing all possibility of the existence of any kind of classification (Fig. 15).

3.5. *Cluster association/FMLDA*

FMLDA analysis was used in order to carry out a more integrative approach, i.e. a more detained factor analysis based classification. It is a way to classify observables, in this case neurons, by finding adequate linear parameter combinations according to which neurons can be classified into separate groups or clusters [20]. In contrast with a separate unifactor analysis which represents the contribution strength of each of the factors included, and analyzed separately, FMLDA analyses the factors in an integrative manner. Any clustering detected by previous unsupervised analyses allow the possibility of investigating clustering association, i.e. identify preliminary clusters where clusters obtained in an unsupervised manner can be associated with the real DN cluster, including the VLL and DML clusters. However, as no individual clusters were identified, the positive results of FMLDA analysis could not be employed for cluster associations. FMLDA analysis showed a positive result for both real and virtual samples, at least with regard to Wilk's lambda, 0.85 ($p < 0.05$) and 0.98 ($p < 0.001$), respectively, but with very weak factor loadings. For the real sample, none of the factor predictors were sufficient to determine clustering i.e. factor loading for every predictor was below 40%. This means that no driving force/forces was/were sifficient to separate one cluster from the centrally located data grouping (Fig. 16 and Fig. 17). In other words, weakly separated clusters shared the same underlying dynamics, which points to a stochastic pseudo/clustering process. For the virtual sample, the situation was similar to that of the real one but with only D_s being a valid parameter (factor load 90%), which is inconsistent with the PCA/factor analysis. Thus, FMLDA indirectly confirmed the absence of any translaminar VLL/DML clustering.

3.6. *Supervised clustering and the cluster identification/feed-forward backpropagation ANN – neuron clustering using neural network – data matrices and training algorithm*

Neurons of the DN are clustered according to their histomorphological and topological features, as expressed and quantified through adequate quantitative parameters, using the MATLAB software/Neural Network Toolbox. The network used was a two-layer feed-forward backpropagation neural network. Data were presented to the network as an input matrix comprised of parameter values and an output/target matrix, i.e. DML/VLL target matrix. The network was trained and used for the neuron classification problem. Clustering was performed on both real and virtual samples.

Even at the stage of virtual sample creation using NAR/NARX ANN, there was a hint of classification failure due to the high performance level of the network (Fig. 18) and the penetration of the VLL neurons into the virtual sample structure. This result indicated a great similarity between these two neuronal populations, but the previously described analysis was necessary for the provision of clarity and completeness concerning the clustering/classification analysis. Indeed, what was presupposed was shown to be the case, the feed-forward backpropagation ANN operating in a supervised learning mode again exhibited a failure to classify DN neurons, thus excluding any chance of cluster identification (Table 4). As can be seen from Table 4, none of the samples showed a correct level of neuron classification (above 80%) for either VLL or DML. Only the real sample of DML neurons was correctly classified (95.1%), but with only 1.3% of VLL neurons correctly classified, this explains

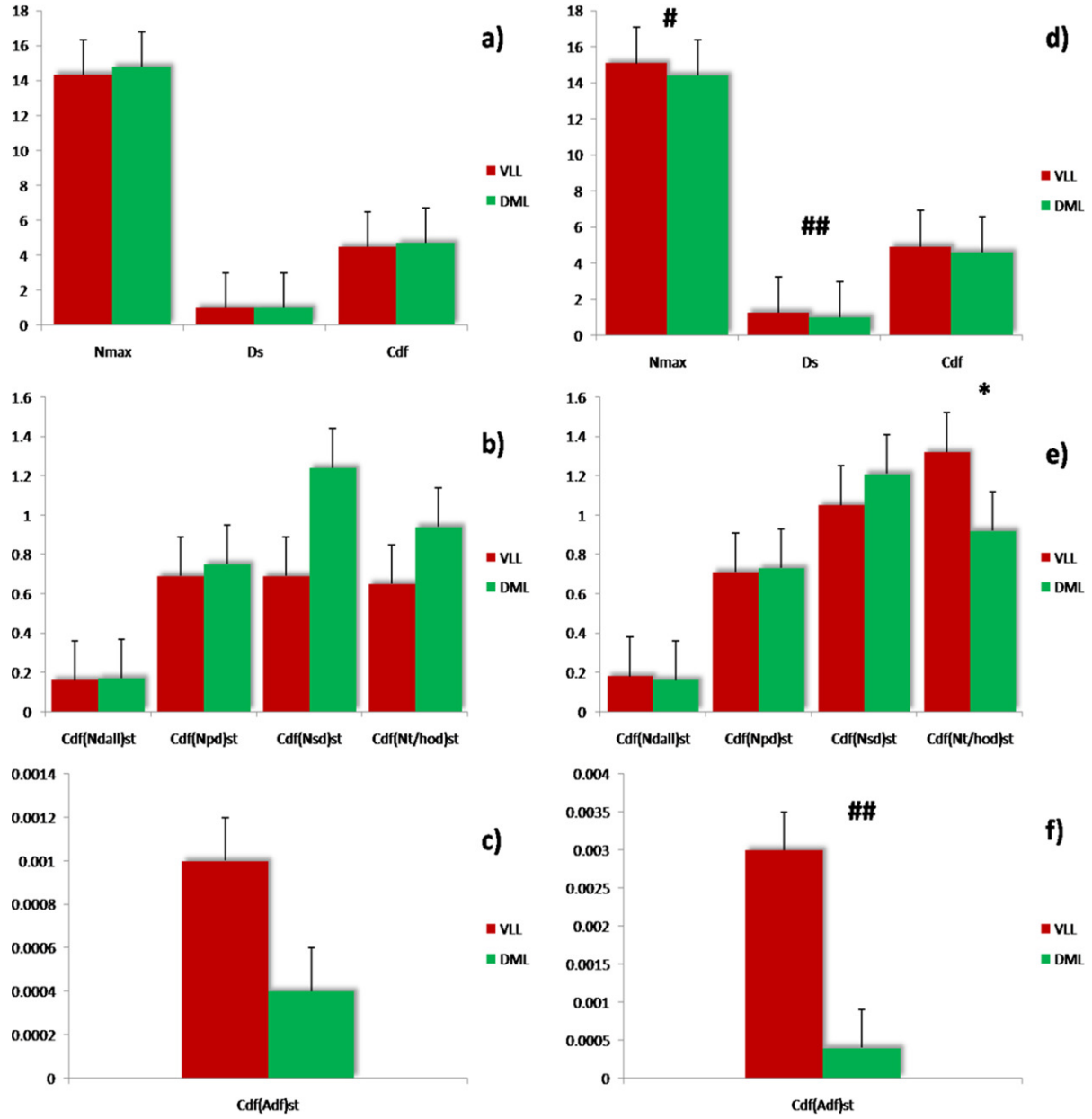

Fig. 11. Morphometric complexity parameters of dendritic arborization of DN neurons; statistically significant ($p < 0.05$); # highly significant ($p < 0.01$); ## very highly significant ($p < 0.001$) adjacent plots with the same parameter sets represent real (red–left) and virtual sample (green–right).

nothing more than the extreme similarity of inter-cluster similarity. Additionally, odds ratios in both cases of VLL and DML were below one, thus confirming the extreme translaminar histological similarity of the topology of these two neuron clusters.

3.7. The integrative decision analysis

Here, the results obtained are summarized and a final statement made concerning the entire outcome of the analysis of the DN neuromorphotopological clustering/classification. Despite the false positivity of the FMLDA analysis, all other analyses, including ether supervised or unsupervised methods, demonstrated the lack of translaminar VLL/DML classification. This confirms the histological similarity of these two topologically and developmentally different neuronal clusters.

4. Discussion

A previous study dealing with the neuromorphotopological classification of DN neurons in the central and border zones [12] showed that these DN neurons could not be histologically classified as two topological neuron subtypes. This led to the further conclusion that the histologically observed DN neuron distribution is uniform throughout the whole gray nuclear mass. However, a subsequent study, similar with the previous one [10], demonstrated strong clustering of the border neuron type into two sub-clusters, i. e., external and internal border neurons. This result complemented the understanding of histological neuron types distributed throughout the nucleus:

Table 2. Data mean ± SD, t- and the p-values for parameters of DN neuron morphology taken from the real sample

Parameters	VLL	DML	t-value	p-value
		Unstandardized parameters		
Surface parameters				
A_s	1143.41 ± 514.32	1230.76 ± 588.18	−1.43	$p > 0.05$
A_n	7170.76 ± 2849.02	7537.64 ± 3118.24	−1.12	$p > 0.05$
A_{dt}	6492.62 ± 2970.59	6368.83 ± 3254.31	0.36	$p > 0.05$
A_{nf}	34824.31 ± 16252.56	38612.1 ± 20360.28	−1.86	$p > 0.05$
A_{df}	28495.26 ± 11270.98	30527.43 ± 14903	−1.39	$p > 0.05$
A_{pns}	21465.24 ± 9741.32	21810.81 ± 12146.71	−0.28	$p > 0.05$
Length parameters				
L	1527.95 ± 605.8	1604.09 ± 665.26	−1.09	$p > 0.05$
r_c	41.25 ± 15.71	40.24 ± 14.93	0.6	$p > 0.05$
r_b	43.15 ± 14.53	45.58 ± 13.44	−1.59	$p > 0.05$
r_t	89.62 ± 23.06	93.32 ± 24.45	−1.42	$p > 0.05$
D_{wdth}	6.75 ± 4.53	6.54 ± 4.98	0.4	$p > 0.05$
Shape parameters				
D_o	1.19 ± 0.36	1.21 ± 0.35	−0.56	$p > 0.05$
M_s	1.19 ± 0.11	1.21 ± 0.11	−1.51	$p > 0.05$
M_n	3.47 ± 2.44	4.68 ± 9.01	−1.61	$p > 0.05$
Branching parameters				
N_{dall}	31.34 ± 11.05	33.24 ± 13.03	−1.43	$p > 0.05$
N_{pd}	7.04 ± 1.86	7.59 ± 2.06	−2.57	$p < 0.05$
N_{sd}	10.7 ± 5.61	12.04 ± 6.83	−1.94	$p > 0.05$
$N_{t/hod}$	13.64 ± 8.38	13.63 ± 9.53	0.006	$p > 0.05$
Complexity parameters				
$N_{\max}$	14.34 ± 4.81	14.78 ± 4.79	−0.84	$p > 0.05$
D_s	1 ± 0.0000001 1 ± 0.03	−0.91	$p > 0.05$	
C_{df}	4.48 ± 4.74	4.7 ± 5.65	−0.39	$p > 0.05$
		Standardized parameters		
Length parameters				
L_{st}	2453.53 ± 1841.51	2659.41 ± 1981.58	−0.98	$p > 0.05$
$(D_{wdth})_{st}$	0.01 ± 0.01	0.01 ± 0.01	−0.1	$p > 0.05$
$(r_c)_{st}$	2.01 ± 2.2	1.7 ± 1.29	1.58	$p > 0.05$
Complexity parameters				
$C_{df}(A_{df})_{st}$	0.001 ± 0.01	0.0004 ± 0.002	0.85	$p > 0.05$
$C_{df}(N_{dall})_{st}$	0.16 ± 0.18	0.17 ± 0.26	−0.44	$p > 0.05$
$C_{df}(N_{pd})_{st}$	0.69 ± 0.77	0.75 ± 1.13	−0.54	$p > 0.05$
$C_{df}(N_{sd})_{st}$	0.69 ± 1.21	1.24 ± 4.52	−1.45	$p > 0.05$
$C_{df}(N_{t/hod})_{st}$	0.65 ± 1.56	0.94 ± 3.65	−0.93	$p > 0.05$

Branching parameters are fractional due to semi-computational NARX-based manner of extrapolation and sample enlargement used for missing values of the real sample.

the histological neuron type corresponding to the external/internal border neuron cluster also corresponded to the portion of the central neurons that exhibit the same morphological properties. Thus, though the histological neuron subtypes are probably scattered inside the central region, what is certain is that they are organized on the border of the nucleus into two sub-clusters, one external and the other internal, with equivalent neuro-functional implications [10]. In this study an attempt was made to try and complete understanding about the distribution of DN neurons. Results have shown that VLL and DML neurons share the same structural properties and that the previous description is complete. The only unknown, is whether the central region has any internal topological compartmentalization, as it is considered to be an unified compartment. What is obvious from previous results is that the only compartmentalization that exists in the DN is an external/internal border neuron neuromorphotopological compartmentalization. Although the neurons belonging to the DML are magnocellular neurons [3], methods of multidimensional analysis have shown that this parameter itself is not sufficient to successfully confirm the classification. Fig. 2 shows two neurons that on first sight appear very different but belong to the two dentate lamina. However, upon a closer examination, DML neurons appear to exhibit more developed dendritic branching and a slightly larger cell body. Even the complexity of the dendritic field is not much greater due to the regularity of dendritic curvature. This, by the way, is just one more example of the relation between quantitative computational studies and qualitative ones where the effectiveness of the quantitative approach is shown once again, especially when combined with the power of multidimensionality. Thus, facts about DML magnocellularity are potentially based upon insignificant interneuron differences in the cell body size or inadequate sample sizes. Maybe a greater number of neurons in this lamina have a larger cell body than neurons in the VLL, but this number is insignificant despite the fact that maybe these large neurons represent DML specific markers that cannot be found in the VLL. Even if this were the case, though the difference in neuron size was not observed in this study, the parameter is not by itself, according to the rules of multidimen-

Table 3. Data mean ± SD, t- and p-values for the parameters of DN neuron morphology taken from the virtual sample

Parameters	VLL	DML	t-value	p-value
		Unstandardized parameters		
Surface parameters				
A_s	1167.77 ± 359.22	1198.37 ± 613.05	−0.97	$p > 0.05$
A_n	7277.84 ± 2471.97	7339.28 ± 3306.01	−0.3	$p > 0.05$
A_{dt}	6626.94 ± 1950.95	6201.23 ± 3369.75	2.46	$p < 0.05$
A_{nf}	36410.85 ± 13059.17	37595.99 ± 21023.27	−1.05	$p > 0.05$
A_{df}	30203.43 ± 10097.69	29724.074 ± 15499.32	0.56	$p > 0.05$
A_{pns}	21994.33 ± 5651.42	21236.84 ± 12485.71	1.38	$p > 0.05$
Length parameters				
L	1629.45 ± 462.6	1561.88 ± 705.09	1.71	$p > 0.05$
r_c	41.39 ± 11.32	39.18 ± 16.09	2.33	$p > 0.05$
r_b	43.53 ± 9.26	44.38 ± 15.15	−1.06	$p > 0.05$
r_t	88.7 ± 15.17	90.86 ± 28.4	−1.57	$p > 0.05$
D_{wdth}	4.72 ± 3.93	6.44 ± 4.96	−5.38	$p < 0.001$
Shape parameters				
D_o	1.41 ± 0.16	1.18 ± 0.39	14.18	$p < 0.001$
M_s	1.19 ± 0.06	1.18 ± 0.22	2.62	$p < 0.01$
M_n	4.38 ± 6.2	4.56 ± 8.92	−0.34	$p > 0.05$
Branching parameters				
N_{dall}	31.51 ± 5.91	32.37 ± 13.92	−1.45	$p > 0.05$
N_{pd}	7.36 ± 1.34	7.39 ± 2.37	−0.28	$p < 0.05$
N_{sd}	9.99 ± 3.84	11.73 ± 7.02	−5.01	$p < 0.001$
$N_{t/hod}$	16.26 ± 4 13.27 ± 9.65	7.37	$p < 0.001$	
Complexity parameters				
$N_{\max}$	15.08 ± 2.9	14.39 ± 5.3	2.6	$p < 0.01$
D_s	1.24 ± 0.1	0.98 ± 0.16	30.28	$p < 0.001$
C_{df}	4.91 ± 2.32	4.58 ± 5.63	1.38	$p > 0.05$
		Standardized parameters		
Length parameters				
L_{st}	2529.58 ± 1334.73	2589.42 ± 2001.24	−0.53	$p > 0.05$
$(D_{wdth})_{st}$	0.006 ± 0.004	0.006 ± 0.01	1.35	$p > 0.05$
$(r_c)_{st}$	1.82 ± 1 1.66 ± 1.31	2.05	$p < 0.05$	
Complexity parameters				
$C_{df}(A_{df})_{st}$	0.003 ± 0.005	0.0004 ± 0.002	7.08	$p < 0.001$
$C_{df}(N_{dall})_{st}$	0.18 ± 0.19	0.16 ± 0.26	0.87	$p > 0.05$
$C_{df}(N_{pd})_{st}$	0.71 ± 0.51	0.73 ± 1.13	−0.29	$p > 0.05$
$C_{df}(N_{sd})_{st}$	1.05 ± 1.84	1.21 ± 4.47	−0.82	$p > 0.05$
$C_{df}(N_{t/hod})_{st}$	1.32 ± 2.07	0.92 ± 3.6	2.17	$p < 0.05$

sional analysis, sufficient to claim the classification exists and is valid only because of that. In this case it is no more than merely a qualitative observation of one neuron population unconfirmed by any quantitative computational multivariate study. Also, in additional support of these findings, Maric [8] found a uniform distribution of all histological and topological neuron types throughout the nuclear lamina, thus pointing to their similarity despite the occurrence of potentially characteristic neuron markers, they were unable to confirm any classification. Braak and Braak [21] reported that the soma of the large neuron generates a great number of dendrites that radiate in all directions when the neuron is located in the central portion of the dentate nucleus. Analogously to this, but more generally, are the results of Fiala and Harris [22], the so called Harris–Fiala pattern. Accordingly, it is an universal fact that large neurons are characterized by both large cell bodies and consequently more elaborative dendritic fields with respect to neuroperikaryion size and vice versa for small granular neurons. Other studies additionally either support or discard this relation as valid for other neuron types. Studies performed on thalamocortical cat neurons using linear regression analysis have shown that cross-sectional area or neurosoma diameter provide a poor predictor of dendritic length. In contrast with this, the number of first order dendrites and the values of their total diameter provide a good estimate of overall size of thalamocortical neurons [23]. The analysis reported here, has not detected the same relations in terms of neurodendritic branching but it has yet to be applied to the other type of neuron. Additionally, a study by Conlee *et al.* [24] reports reduction of neuron size in parallel with reduction of dendritic length in the medial superior olive of stressed albino rabbits. Though this wasn't the case for all parts, these results represent an excellent example of adaptive morphological changes taking place in neurons [24]. Although these are counter examples, this study also suggests that constructive adaptation can be expected as well, provided of course, there is an adequate neurostimulatory environment. As the largest portion of both laminar samples employed for this study were comprised of central neurons the correlation obviously may contribute to a false picture of DML magnocellularity. Experience with the correlation–comparison analysis has shown that though some neuromorphological parameters are in a particular correlational relationship, this does not necessarily mean that such parameters are significantly different between the

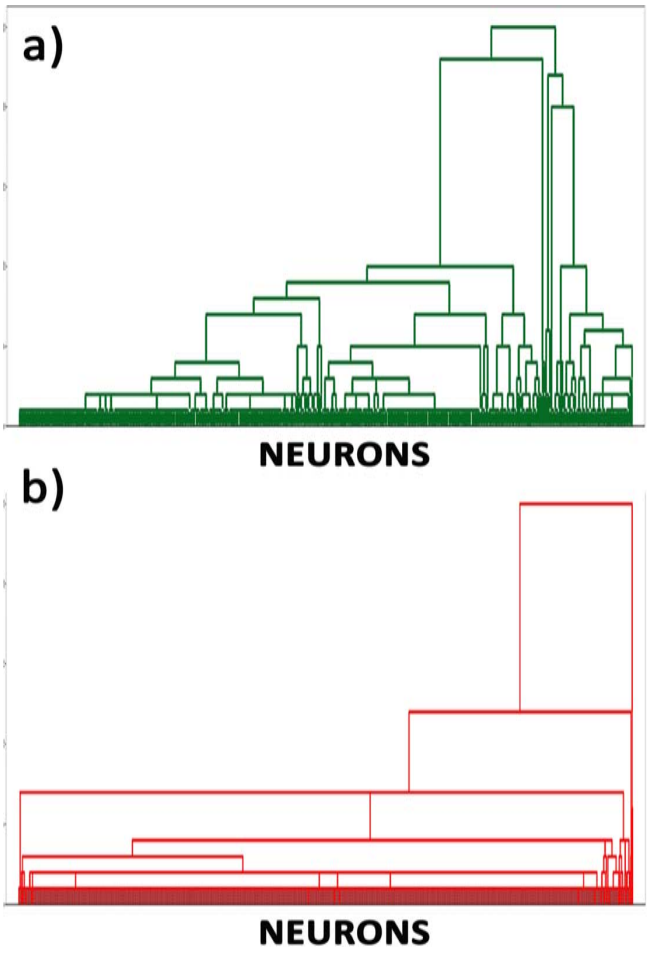

Fig. 12. Dendrogram of the hierarchical cluster analysis of DN neurons. (a) Real sample case. The two main clusters are very similar to each other thus eliminating the possibility of any successful clustering. DN neurons to the left represent the insignificant third cluster of the outliers identified by the *k*-means cluster analysis. (b) Virtual sample case. Although the situation is a little bit different to that of the real sample, with a smaller number of subclusters, the two main pseudo/clusters are even closer than they are for the case of the real sample, thus confirming the absence of neuromorphological DN classification in terms of topological criteria (axes signify the individual numbered neurons).

samples, i.e. one of them might be, but the other one does not have to be, significantly different. Thus, the significantly greater dendritic arborization area of the DML neuron does not necessarily lead to significantly larger cell bodies in the DML sample. Results supporting this line of reasoning include those reported here, along with results reported by Mihajlović and Zěcević [7] and Maric [8] that show independent dendritic morphology and did not confirm any pattern of dendrite/perikaryon dependence. To summarize, the DML/VLL magno/parvocellularity originates from insignificant qualitatively based interneuron differences of perikaryon size and/or an insignificant number of such neurons. Either way, they are not convincing enough to support the DML/VLL DN neuron classification. This is additionally supported by Mihajlovicć and Zecevicć [7] and Hayaran *et al.* [25] who found that asymmetrical and fusiform neurons are ubiquitous neuronal types that uniformly invade both laminae and make them the dominant neuronal populations. Similarly, but with histologically different neuron types, are the results of Hayaran *et al.* [25], that human adult dentate nucleus is only comprised of large multipolar neurons. Very probably, during the first stages following formation of specific laminar neuron types, these differences are sustainable but with the later development of the VLL after gestation week 19, either a very small portion of DML neurons become more like VLL neurons Mihajlović and Zecević [7], or some neural migrations are still occurring with uniform effect upon neurons belonging to these two lamina. As shown by Conlee *et al.* [24], neural synaptic adaptation may even be sufficient to shape these neurons similarly in the adult brain. However, the results of some studies [7, 25–31], also support the analyses reported here by not showing marks and indicators of neuron compartmentalization besides those of structural differentiation of neuron precursors that determine nucleus function. Thus, ether embryonic scenario may lead to the uniformity of neurons reported for the adult DN. The virtual sample showed some additional inter-neuron differences but due to the low performance rate of the feed-forward network caused by an absence of differences, such results are suspicious and rate validity lower in terms of precise specification differences. But the results obtained for the virtual DN sample have full and legitimate validity concerning the confirmation of complete absence of a translaminar DML/VLL DN neuron classification as previously has already been shown for the real sample.

Though some positive conclusions, based upon the results of separate unifactor analysis, could be proposed, in conclusion it can be said that DN neurons cannot be classified into VLL/DML neuromorphotopological subtypes. Although some differences exist they are not sufficient to support any classification. The methods of multidimensional statistical analysis are once again shown to be the best for such difficult tasks.

Appendix

A.1. The neuron surface parameters

Expressed in squared microns (μm^2), the neuron surface parameters determine various aspects of surfaces and compartments of a neuron's 2D binary image. These parameters represent the size of neuron and its various compartments. They include: a) Surface area of the entire neuron (A_n), b) Surface of the neurosoma/perikaryon (A_s) [32], c) Surface area of the dendritic tree of a neuron (A_{dt}), d) Surface area of neuron field (A_{nf}), e) Surface area of dendritic field (A_{df}), and f) Surface area of perineuronal space (A_{pns}). The A_n parameter represents the actual real surface of the entire area of a neuron's 2D binary image (Fig. A.1a). Values for a particular neuron are obtained by direct computational measurement analysis of the neuron image (Image J software). The A_s parameter defines the actual real surface of a neuron perikaryon image after digital removal of dendrites (Fig. A.1a).

Like A_n, A_s is also directly measured and the value obtained in pixels is converted to squared micrometers. A_{dt} gives the actual real surface of the neuronal dendritic tree following digital removal of the perikaryon. This parameter is derived from the difference between A_n and A_s:

$$A_{dt} = A_n - A_s. \tag{A.1}$$

A_{nf} represents a surface of the minimal radial field occupied by a neuron image. It is obtained by measuring the surface of the

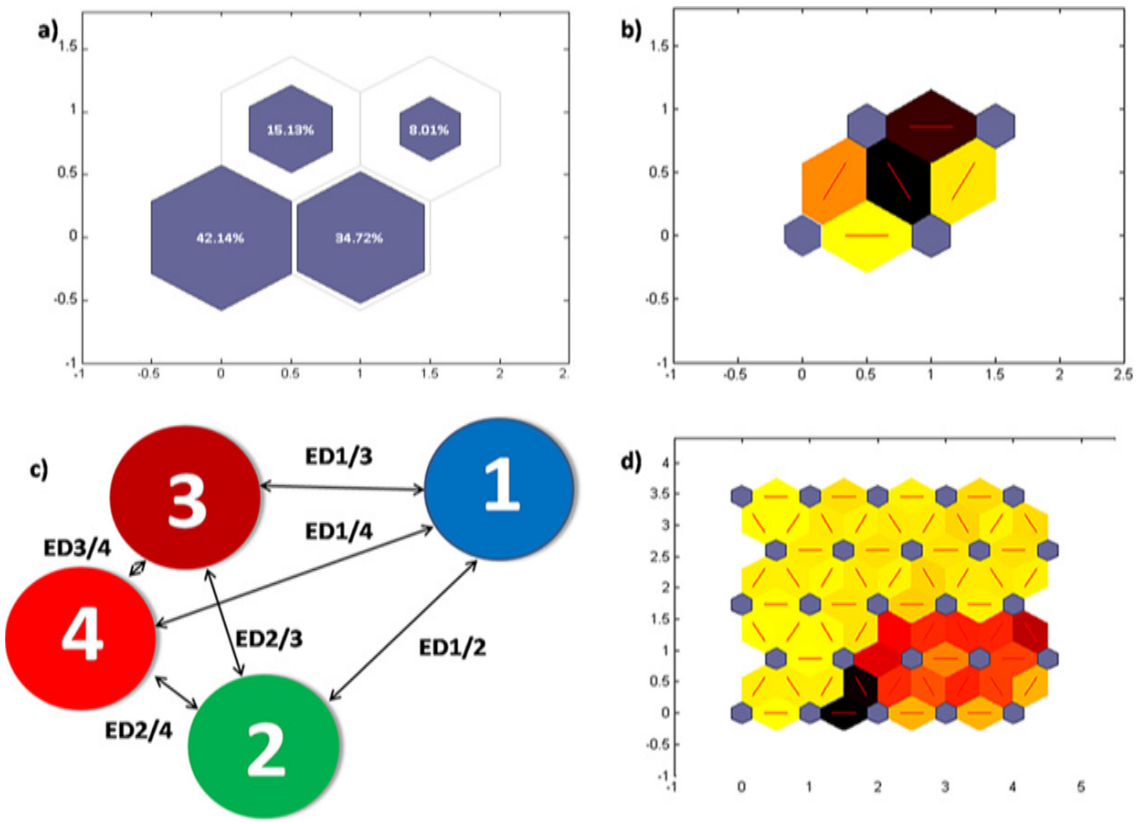

Fig. 13. Kohonen's SOM ANN classification output for the natural DN neuron sample. (a) Percent of DN neurons belonging to each cluster – it can be seen that the third SOM cardinal neuron representing cluster III (lower left) carries the greatest number of DN neurons while the second neuron/cluster (upper right) includes the least. Potential association of either cluster III or IV with one of the other two clusters would have resulted in successful classification. (b) Inter-cluster Euclidian distances (ED) – ED1/4 > ED1/2 > ED1/3 > ED2/3 > ED2/4 > ED3/4. ED2/3 is calculated in a semicomputational manner based on the others. Graph shows the previous assumption fails as clusters II–IV are very close to each other. (c) Reconstruction of the inter-cluster relations shows the obvious failure of the DN classification as cluster I carries less than 30% of the DN neurons (see explanation in text). (d) SOM five-rank artificial neuron matrix confirms DN classification failure – the lower right more distant sub-clusters (outliers) are dispersed and terminal, i.e. do not represent the separation zone between clusters of closer neurons (yellow colored ED distances) representing the one and only one single cluster (major upper left artificial neuron cluster).

Table 4. Confusion matrix of feed-forward backpropagation ANN performance for neuromorphotopological clustering of DN neurons

Neuron type	% of correctly classified neurons	% of misclassified neurons	Classification ratio	Modified odds ratio
		The real DN sample		
VLL	1.3	98.7	0.01	0.26
DML	95.1	4.9	19.41	
		The virtual DN sample		
VLL	64.4	35.6	1.81	0.88
DML	32.6	67.4	0.48	

polygon outlining a neuron image with the tips of the dendrites as its vertices (Fig. A.1b). A_{df} gives the surface of the minimal radial field occupied by a dendritic tree image after the perikaryon has been digitally removed. This value is calculated as the difference between A_{nf} and A_s:

$$A_{df} = A_{nf} - A_s. \tag{A.2}$$

A_{pns} gives the inter-dendritic surface, i.e. the surface between the dendrites. It is obtained from the A_{nf} polygon after the whole neuron has been digitally removed. It is calculated as the difference between A_{nf} and A_n:

$$A_{pns} = A_{nf} - A_n. \tag{A.3}$$

Since the perineuronal space is filled with neuroglial cells, as well as axon bundles, dendrites and small interneurons [1], A_{pns} might be thought of as a partial neuromorphological measure of neuroglial connectedness and supportiveness or from neurophysiological aspect it can be interpreted as the partial neurotrophic strength of the particular neuron. These surface parameters are all unstandardized.

A.2. *Neuron shape parameters*

All neuron shape parameters are also unstandardized. They measure and determine various aspects of neuron shape as well as its compart-

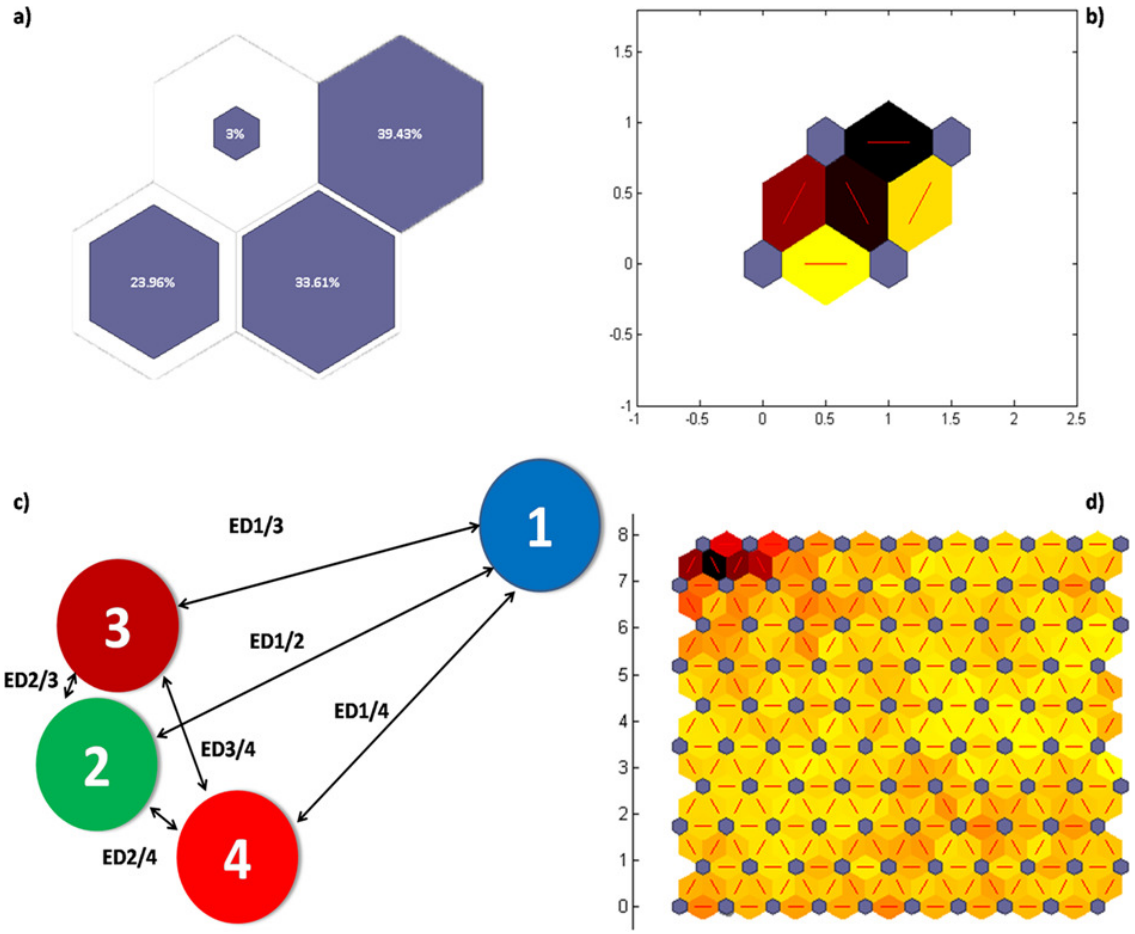

Fig. 14. Kohonen's SOM ANN classification output for the virtual DN neuron sample. For all four panels the outcome is the same as the real sample case, thus leading to the same conclusion as for cluster/neuron 1 as insufficient to support the classification.

ments from a neuron's 2D binary image, including: a) The fractal dimension of a neuron's 2D binary image outline (D_o), b) The index of asymmetry of a neuron (M_n), and c) The index of the somatic asymmetry (M_s). D_o gives a quantitative computational measure of the real shape of a neuron. It is obtained by the box-counting method where the outline of a digital 2D B&W neuron image is sequentially covered by squares with discretized edge/diameter values, i.e. with boxes of different precisely defined sizes calculated by a base two geometrical progression. The number of squares is plotted against the diameter values and fit by a first-order polynomial. The graph slope coefficient gives the value of D_o (Fig. A.2a and A.2c).

M_n is a measure of the inverse circularity of the shape of a neuron. It reflects a neuron's roundness and compactness of shape and is calculated from:

$$M_n = \frac{PR_N^2}{4\pi \cdot A_n} \tag{A.4}$$

where PR_N gives the perimeter of the pericaryodendritic/general somatic compartment. It is also equivalent to the asymmetry index of the dendritic field (M_{df}) if the statistical difference between M_{df} and M_n is not significant ($p > 0.05$). M_{df} provides the majority of shape variance due to large interneuronal variation in the shape of the dendritic tree and the M_n variance primarily depends upon it. M_s gives the inverse circularity of the neurosomatic shape and is equivalent to M_n. Its value is obtained using the same formula after digitally removing the dendrites:

$$M_s = \frac{PR_S^2}{4\pi \cdot A_s} \tag{A.5}$$

where PR_S becomes the perimeter of a neurosoma without dendrites.

A.3. Unstandardized compartmental neuron length parameters

Expressed in microns (μm), the unstandardized compartmental neuron length determines the length of various aspects and compartments of a neuron's 2D binary image morphology. These are, a) Total dendritic length (L), b) Radius of the circle with the maximal number of intersections with dendrites (r_c), c) Radius of the circle with the maximal number of intersections with dendritic branching points or radius of the maximal number of dendritic branches (r_b), d) Radius of the circle with the maximal number of intersections with dendritic terminating points or radius of the maximal number of dendritic terminations (r_t), and e) Average dendritic width (D_{wdth}). L gives the sum of all dendritic lengths [33, 34]. It is obtained from a skeletonized neuron's 2D binary image after digital removal of the perikaryon, i.e. on a dendritic tree image. The surface of such an image is actually L as the dendrite width is reduced to one pixel. The

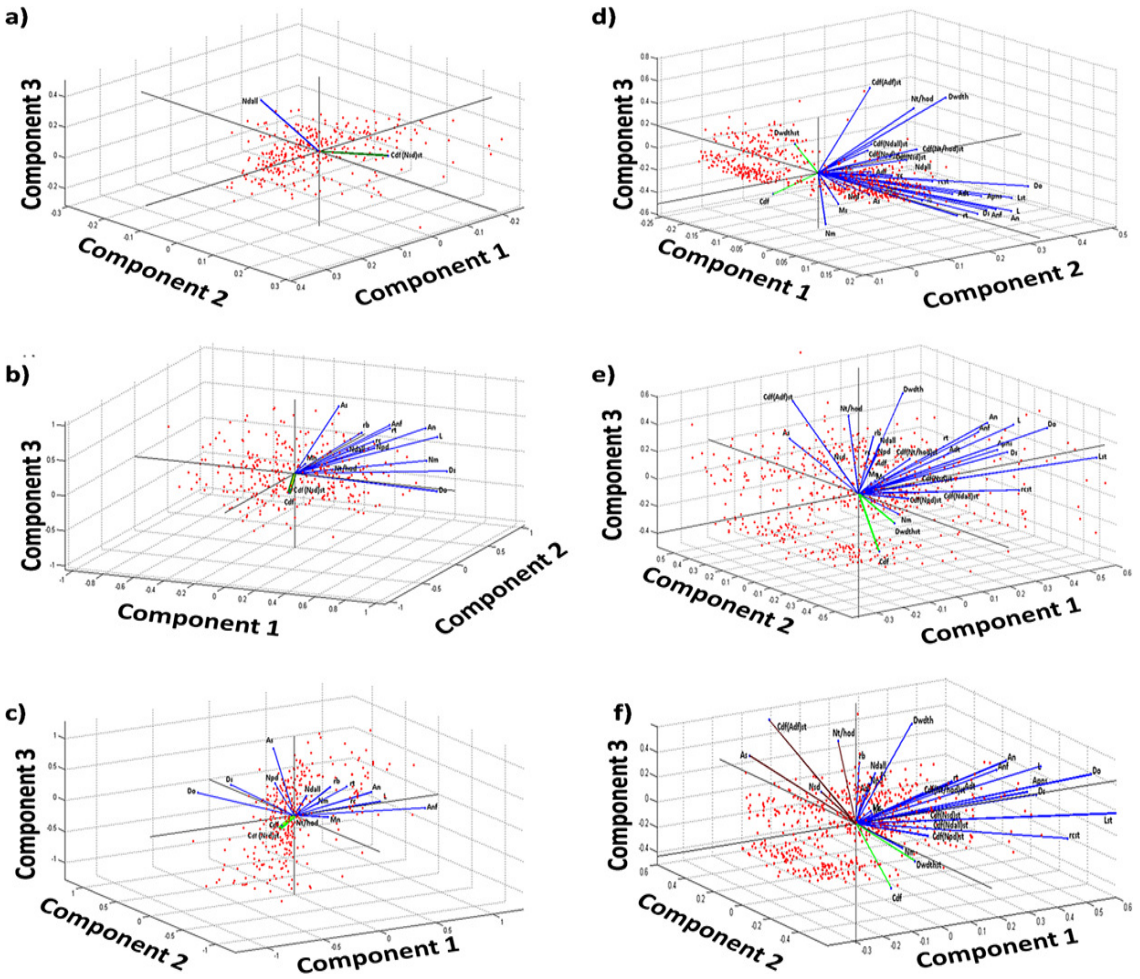

Fig. 15. PCA/FA for real and virtual DN neuron datasets. Graphs (a)–(c) Real neuron data sample. (a) PCA analysis, (b) FA with the varimax rotation, and (c) FA with promax rotation. Graphs (d)–(f) Virtual neuron data sample. (d) PCA analysis, (e) FA with varimax rotation and (f) FA with promax rotation. PCA/FA analysis of virtual sample shows three highly irregular and variable inter-analytically observed pseudo/clusters while real sample data are grouped into a single cluster. Colors of driving forces/factor predictors indicate direction and location of potential pseudo/clusters with respect to others – Graphs show the high level of the cluster-matter inconsistency, thus contesting the DN translaminar or any other classification. It is interesting to note arrangement of the three-cluster solution on panels (d) and (f).

position of the maximal dendritic arborization density is given by r_c, which represents the radius of the circle that has the maximum number of intersections with dendrites (empirically $N_{\max}$) [32]. It is obtained with a MATLAB plug-in (FRACT8) created by the authors for digital image processing and analysis. In short, when the fifth-order polynomial fitting, necessary for calculation of C_{df}, is obtained, the value of r_c is obtained in a retrograde manner (Fig. A.3). Thus the value of r_c is obtained computationally from the theoretical fifth-order polynomial interpolation giving $N_{\max}$. It can be considered a partial complexity parameter as it is related very closely with $N_{\max}$. In contrast to r_c, r_b and r_t are non-theoretical parameters obtained directly from image analysis (Fig. A.3).

D_{wdth} gives the average dendritic width. It is obtained as the following ratio:

$$D_{wdth} = \frac{A_{dt}}{L}. \tag{A.6}$$

A.4. *Standardized compartmental neuron length parameters*

All standardized compartmental neuron length parameters are standardized to A_s. This eliminates variation and the dependence of the compartmental length upon the size of a neuron's soma and comparisons become more accurate for the unifactor analysis. They are: a) Standardized total dendritic length (L_{st}), b) Standardized radius of the *NMAX* circle ($(r_c)_{st}$), and c) Standardized average dendritic width ($(D_{wdth})_{st}$). They are calculated as:

$$L_{st} = \frac{L^2}{A_S}, \tag{A.7}$$

$$(r_c)_{st} = \frac{r_c^2}{A_S}, \tag{A.8}$$

$$(D_{wdth})_{st} = \frac{D_{wdth}^2}{A_s} \tag{A.9}$$

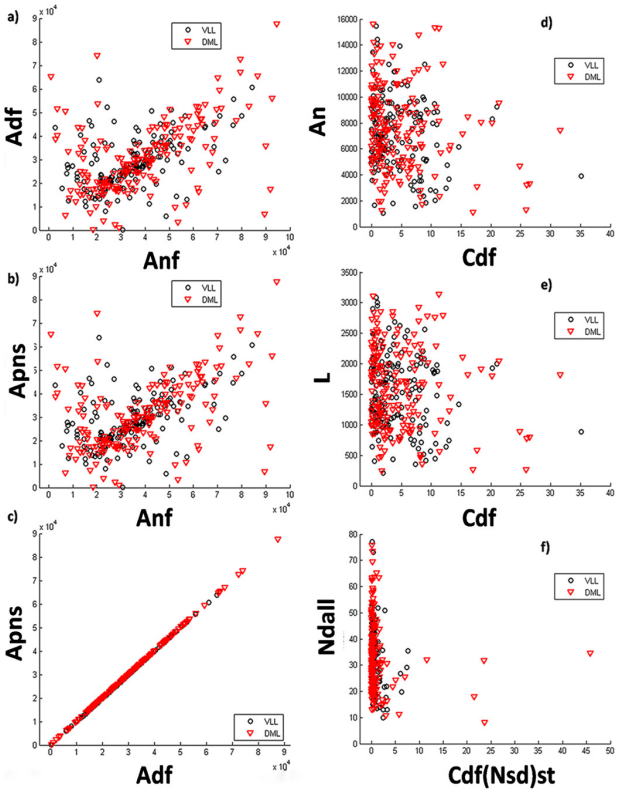

Fig. 16. FMLD 2D two-factor scatter plot of the natural DN neuron sample dataset. Graphs (a)–(c) illustrate 2D presentations with dimensionality reduction of the DN neuron dataset for combinations of all three NMF-based attractor factors, Anf, Adf, and $Apns$. Graphs (d)–(f) illustrate 2D presentations with dimensionality reduction of the DN neuron dataset for some of the PCA/FA-based dominant predictor classifiers, Cdf vs. An, Cdf vs. L and $Cdf\ (Nsd)st$ vs. $Ndall$. None of the six plots confirm existence of DN translaminar VLL/DML clustering (it is of interest to note the similarity between (a) and (b)).

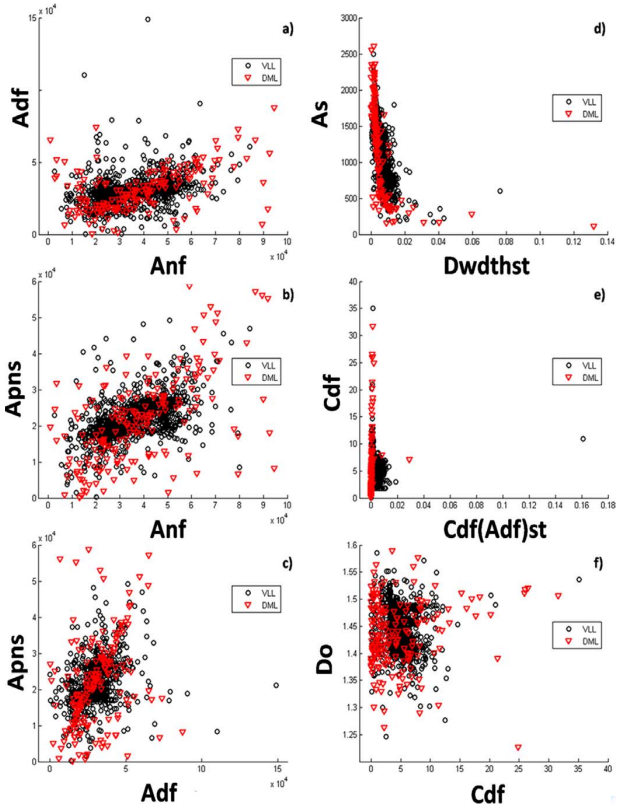

Fig. 17. FMLDA 2D two-factor scatter plot of the virtual DN neuron sample dataset. Graphs (a)–(c) illustrate 2D presentations with dimensionality reduction of the DN neuron dataset for combinations of all three NMF-based attractor factors, Anf, Adf, and $Apns$. Graphs (d)–(f) illustrate 2D presentations with dimensionality reduction of the DN neuron dataset for some PCA/FA-based dominant predictor classifiers, $(Dwdth)st$ vs. As , $Cdf\ (Adf\ )st$ vs. Cdf and Cdf vs. Do. None of the six plots confirm the existence of DN translaminar VLL/DML clustering (it is of interest to note the similarity between (a) and (b)).

A.5. Unstandardized dendritic arborization branching parameters

The unstandardized dendritic arborization branching parameters number neuron dendrites, they are: a) Number of primary dendrites (N_{pd}), b) Number of secondary dendrites (N_{sd}), c) Number of tertiary dendrites (N_{td}), d) Total number of tertiary and higher order dendrites ($N_{t/hod}$), and e) Total number of all dendrites (N_{dall}) (Fig. A.4). N_{pd} counts the dendrites originating directly from the soma, i.e. primary dendrites. N_{sd} gives the number of second order dendrites, i.e. dendrites formed by branching of the first order dendrites or primary branching (Fig. A.4). N_{td}I gives the number of tertiary order dendrites, i.e. dendrites formed by second order dendritic branching or secondary branching. $N_{t/hod}$ represents the sum of the tertiary and higher order dendrites. Finally, N_{dall} is the number of all dendrites of a neuron. The different orders of branching are not employed as parameters in this study.

A.6. Unstandardized neuromorphological complexity parameters

The unstandardized neuromorphological complexity parameters are the most important group of morphological parameters for describing morphological features of a neuron. However, this does not mean that significant internuclear differences are necessarily accounted for in terms of these parameters. Neuromorphological complexity as shape and the detailed complexity of a neuron's image can be reduced to branching pattern complexity [35], but it is highly dependent on the branching characteristics and order (expressed through the branching parameters) and the topological orientation of a neuron in 2D space. Thus, a dendritic tree can be symmetric or asymmetric and thus less or more complex in its branching degree when this is balanced in a more or less radial manner or when viewed from different perspectives. To capture and quantify all possible neuromorphological complexity and variation, originating mainly from variations in dendritic branching pattern complexity, four integrative unstandardized complexity parameters of neuron morphology are defined here. They are: a) Fractal dimension of a skeletonized neuron image (D_s) [36], b) Maximal complexity index of dendritic arborization density ($N_{\max}$) [32, 34], and c) Dendritic branching pattern complexity (C_{df}). D_s represents a fractal dimension of the skeletonized neuron image reduced to the width of one pixel (Fig. A.2b and A.2c). On such an image dendrites preserve the same length as in the original image while a neuron body, due to its radial symmetry, is reduced to one pixel. Thus, it can be also said that D_s selectively

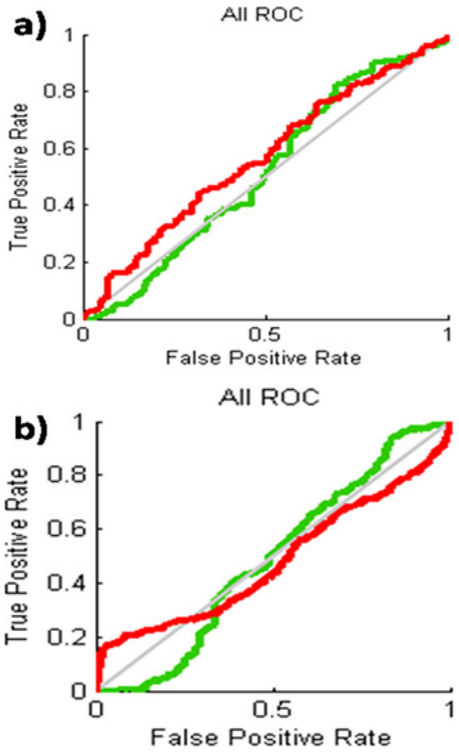

Fig. 18. ROC curve of feed-forward backpropagation ANN performance for the task of neuromorphotopological supervised clustering of DN neurons. (a) Real sample case, (b) Virtual sample case. In both cases graph shows very low network performance thus pointing to the absence of any kind of DN classification.

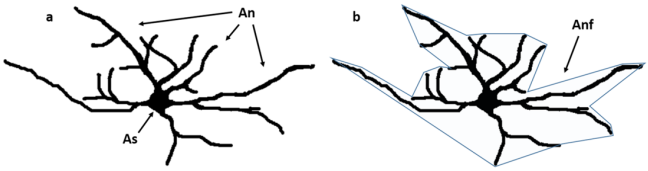

Fig. A.1. Graphical representation of the three surface parameters, namely *An*, *As* and *Anf*.

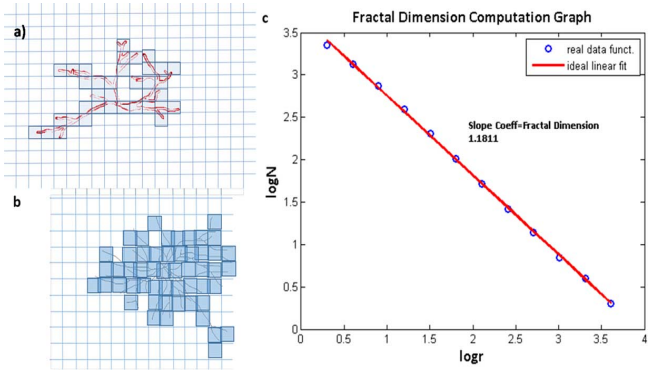

Fig. A.2. Calculation of the fractal *Dn* and *Ds* parameters. Diagram illustrates the principle and application of the fractal box-counting method employed for calculation of parameter values. *N*-number of boxes/squares covering a neuron image of specific side/diameter value (*r*).

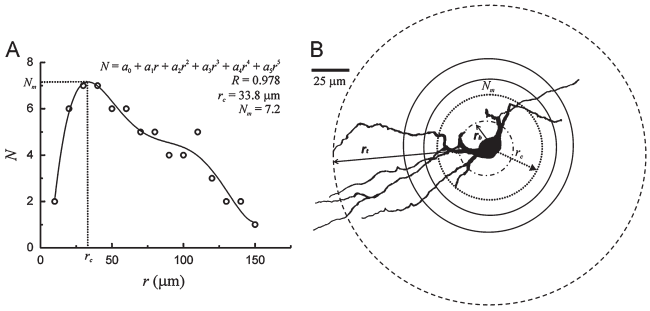

Fig. A.3. Calculation of neuromorphological complexity parameters. The diagram illustrates a modified Sholl's analysis where *rc*, *Nmax*, and Cdf are calculated when the distribution of the number of cross-sections between the circles of a discretized radius and dendritic arbor is fit by a fifth-order polynomial. *rb* and *rt* are also given as non-theoretical parameters obtained by direct analysis of a neuron's 2D binary image.

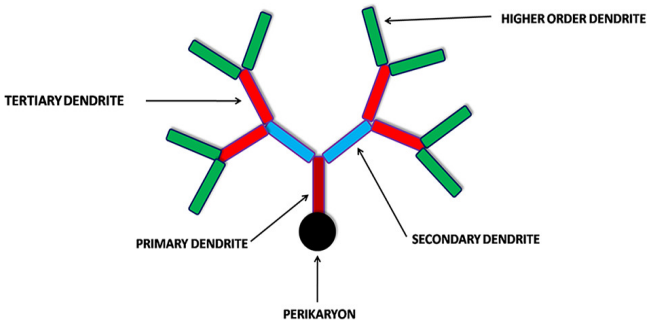

Fig. A.4. Dendritic branch ordering. A higher order is assigned to the terminal dendrites and their branches.

reflects just dendritic branching pattern complexity, i.e. the degree of dendrite arborization curvature. It is also calculated using the fractal box-counting method. The values of $N_{\max}$, r_c, and C_{df}s are obtained following a fractally modified Sholl analysis where a neuron's 2D binary image is overlaid with concentric circles of predefined radii and centered at the geometrical center of the soma. The circle with the minimal/maximal number of dendritic intersections determines the value of $N_{\max}$ and the radius of the $N_{\max}$ circle gives r_c (Fig. A.3). It should be mentioned that values of $N_{\max}$ are theoretical, obtained retrogradely from the fifth polynomial fitting used for calculation of C_{df}. C_{df} is the most integrative of all the three parameters describing the complexity of neuronal shape as it combines $N_{\max}$, D_s, r_c, and similar values, i.e. intermediate N values lying in the $N_{\max}$–$N_{\min}$ range ($N_{\min}$ is not used in this study). It is obtained in a fractal-like manner when the number of intersections between dendrites and circles with predefined radius values, plotted against one another, are fit with the fifth-order polynomial on the basis of its match with the bell-shaped function of the real data. Analogously with the fractal algorithm, the first coefficient is taken as a measure of C_{df} (Fig. A.3).

A.7. Standardized neuromorphological complexity parameters

As the most important parameter, C_{df} is associated with the largest number of standardizations introduced in this study. As significant inter-nuclear differences are expected, neurons must be matched in terms of many parameters so as comparison of the values obtained for C_{df} give valid results. The C_{df} $(A_{df})_{st}$ parameter is calculated

as:

$$C_{df}(A_{df})_{st} = \frac{C_{df}}{A_{df}} \cdot k, \tag{A.10}$$

where k is an arbitrary constant. In correspondance with this, other parameters in this group are $C_{df}\ (N_{dall})_{st}$, $C_{df}\ (N_{pd})_{st}$, $C_{df}(N_{sd})_{st}$, and $C_{df}\ (N_{t/hod})_{st}$. It can be seen that C_{df} is predominantly standardized as branching parameters provide its major determinants.

Acknowledgments

This study was supported by the Ministry of Education, Science and Technological Development, Republic of Serbia, project number III41031. The corresponding author also would like to use this opportunity to thank his personal friend and colleague Dr Goran Platisa, specialized in neurology, whose suggestions about digital image processing were of immense value.

Conflict of Interest

All authors declare no conflicts of interest.

References

[1] Hámori J (1978) Cerebellar dentate nucleus. Organization, cytology and transmitters: V. Chan-Palay (Springer, Berlin-Heidelberg-New York, 1977, 548 p., 293 figs., DM 239.-). *Clinical Neurophysiology* **44(6)**, 795-796.

[2] Mathiak K, Hertrich I, Grodd W, Ackermann H (2002) Cerebellum and speech perception: a functional magnetic resonance imaging study. *Journal of Cognitive Neuroscience* **14(6)**, 902-912.

[3] Mihajlovic P, Zecevic N (1986) Development of the human dentate nucleus. *Human Neurobiology* **5(3)**, 189-197.

[4] Maric D (2010) The quantitative and the qualitative analysis of neurons of the adult human dentate nucleus. *PhD thesis, Novi Sad*.

[5] Grbatinić I, Rajković N, Milošević N (2018) Computational RSM modelling of dentate nucleus neuron 2D image surface. *Computer Methods in Biomechanics and Biomedical Engineering: Imaging & Visualization* **6(1)**, 43-50.

[6] Grbatinić I, Milošević N (2016) Classification of adult human dentate nucleus border neurons: Artificial neural networks and multidimensional approach. *Journal of Theoretical Biology* **404**, 273-284.

[7] Stilling B (1846) *Untersuchungen über den Bau und die Verrichtungen des Gehirns*. Druck und Verlag von Friedrich Mauke.

[8] Gans A (1924) Beitrag zur kenntnis des aufbaus des nucleus dentatus aus zwei teilen, namentlich auf grund von untersuchungen mit der eisenreaktion. *Zeitschrift für die gesamte Neurologie und Psychiatrie* **93(1)**, 750-755.

[9] Hayaran A, Wadhwa S, Bijlani V (1993) Expression of substance P in dentate nucleus of human cerebellum. *Neuroscience Letters* **152(1, 2)**, 99-102.

[10] Yamaguchi K, Goto N (1997) Three-dimensional structure of the human cerebellar dentate nucleus: a computerized reconstruction study. *Anatomy and Embryology* **196(4)**, 343-348.

[11] Schierhorn V, Doedenes K, Nagel I (1977) Quantitative studies on the comparability of neurohistological results in rat cortical pyramids produced by different Golgi methods (author's transl). *Journal Fur Hirnforschung* **18(5)**, 423-429.

[12] Grbatinić I, Marić DL, Milošević NT (2015) Neurons from the adult human dentate nucleus: Neural networks in the neuron classification. *Journal of Theoretical Biology* **370**, 11-20.

[13] Sra S, Dhillon IS (2006) Generalized nonnegative matrix approximations with Bregman divergences. In, Dhillon IS(Eds.)*Advances in Neural Information Processing Systems*(pp. 283-290). Austin, Tx., Computer Science Dept., Univ. of Texas at Austin.

[14] Tandon R, Sra S (2010) Sparse nonnegative matrix approximation: new formulations and algorithms. *Rapport Technique* **193**, 38-42.

[15] Everitt B, Hothorn T (2011) *An Introduction to Applied Multivariate Analysis with R*. New York, Springer.

[16] Kohonen T (1989) *Self-organization and associative memory*. Berlin, Springer-Verlag.

[17] Johnson R, Wichern D (1992) *Applied Multivariate Statistical*. Englewood Cliffs, NJ: Prentice Hall.

[18] Sultan F, Bower JM (1998) Quantitative Golgi study of the rat cerebellar molecular layer interneurons using principal component analysis. *Journal of Comparative Neurology* **393(3)**, 353-373.

[19] Yelnik J, Percheron G, Francois C, Burnod Y (1983) Principal component analysis: a suitable method for the 3-dimensional study of the shape, dimensions and orientation of dendritic arborizations. *Journal of Neuroscience Methods* **9(2)**, 115-125.

[20] McLachlan GJ (1993) Discriminant analysis and statistical pattern recognition. *Technometrics* **35(3)**, 324-326.

[21] Braak H, Braak E (1983) Morphological studies of local circuit neurons in the cerebellar dentate nucleus of man. *Human Neurobiology* **2(2)**, 49-57.

[22] Fiala JC, Harris KM (2008) Dendrite structure. In, Stuart G, Spruston N and Haüsser M (eds.)*Dendrites*(pp. 1-34). Oxford, Oxford University Press.

[23] Havton L, Ohara P (1994) Cell body and dendritic tree size of intracellularly labeled thalamocortical projection neurons in the ventrobasal complex of cat. *Brain Research* **651(1, 2)**, 76-84.

[24] Conlee JW, Parks TN, Creel DJ (1986) Reduced neuronal size and dendritic length in the medial superior olivary nucleus of albino rabbits. *Brain Research* **363(1)**, 28-37.

[25] Hayaran A, Wadhwa S, Bijlani V (1992) Cytoarchitectural development of the human dentate nucleus: a Golgi study. *Developmental Neuroscience* **14(3)**, 181-194.

[26] Murafushi K (1974) Normal development and dysgenesis of the dentate nucleus and inferior olive. *Acta Neuropathol* **27(4)**, 317-328.

[27] Rakic P, Sidman RL (1970) Histogenesis of cortical layers in human cerebellum, particularly the lamina dissecans. *Journal of Comparative Neurology* **139(4)**, 473-500.

[28] Verbitskaya L (1969) Some aspects of the ontophylogenesis of the cerebellum. In, R. Llinas (eds.) *Neurobiology of Cerebellar Evolution and Development* (pp. 859-874). Chicago, American Medical Association.

[29] Wadhwa S, Bijlani V (1988) Cytodifferentiation and developing neuronal circuitry in the human lateral geniculate nucleus. *International Journal of Developmental Neuroscience* **6(1)**, 59-75.

[30] Wadhwa S, Gopinath G, Bijlani V (1985) Nissl & Golgi analysis of the developing human cerebellar nuclei in the early prenatal period. *The Indian Journal of Medical Research* **81**, 193-201.

[31] Zecevic N, Mihajlovic P, Jovanovic D, Rakic L (1986) Cellular characteristics of the development of nucleus dentatus. *Medicinski Pregled* **39**, 553-557.

[32] Milošević NT, Ristanović D, Marić DL, Rajković K (2010) Morphology and cell classification of large neurons in the adult human dentate nucleus: a quantitative study. *Neuroscience Letters* **468(1)**, 59-63.

[33] Ristanović D, Krstonošić B, Milošević NT, Gudović R (2012) Mathematical modelling of transformations of asymmetrically distributed biological data: An application to a quantitative classification of spiny neurons of the human putamen. *Journal of Theoretical Biology* **302**, 81-88.

[34] Ristanović D, Milošević NT, Stefanović BD, Marić DL, Rajković K (2010) Morphology and classification of large neurons in the adult human dentate nucleus: a qualitative and quantitative analysis of 2D images. *Neuroscience Research* **67(1)**, 1-7.

[35] Pantic I, Harhaji-Trajkovic L, Pantovic A, Milosevic NT, Trajkovic V (2012) Changes in fractal dimension and lacunarity as early markers of UV-induced apoptosis. *Journal of Theoretical Biology* **303**, 87-92.

[36] Ristanović D, Milošević NT, Stefanović IB, Marić D, Popov I (2009) Cell image area as a tool for neuronal classification. *Journal of Neuroscience Methods* **182(2)**, 272-278.